

Localization Dynamics and Gauge Theories from Mobile Quantum Impurities

Ephraim Bernhardt, Fan Yang and Karyn Le Hur

CPHT, CNRS, École Polytechnique, Institut Polytechnique de Paris, Route de Saclay, 91128 Palaiseau, France

We study the interplay between superfluid Meissner response, localization dynamics from impurities and gauge theories. The superfluidity is formed in the rung-Mott phase of the bosonic ladder model producing spin-Meissner currents induced by a $\mathbb{U}(1)$ gauge field or a uniform magnetic field. Impurities are described through two-state systems which act as a two-peak random potential. An impurity sits either at the top or at the bottom of the ladder on each rung equally, producing a telegraph signal. The impurities-matter coupling gives rise to an intrinsic \mathbb{Z}_2 gauge theory. Through analytical approaches and numerical exact diagonalization, we address both the weakly-coupled and strongly-coupled rungs limits for impurities. In the weakly-coupled rungs situation, we find a smooth power-law localization whereas the strongly-coupled rungs limit produces a steep localization or insulating phase for various configurations of the potential. We describe the superfluid response relying on quantum spin models showing four-particles coupling in the strongly-interacting regime with impurities and linking with the persistent current limit. Through entanglement and bipartite fluctuation measures, we also identify a many-body localization regime in time after a quench of the system when prepared in a Néel state.

CONTENTS

References

22

I. Introduction	1
II. The model	2
A. Rung-Mott Phase and Definitions	3
III. Weakly-Coupled Rung Limit	4
A. Meissner Effect with Static Impurities	4
B. Meissner Effect with Mobile Impurities	5
C. Strong Interactions with Impurities	6
IV. Strongly-Coupled Rungs Model	8
A. Rotation of the Hamiltonian	8
B. The persistent current limit	9
C. Jordan-Wigner Transformation	9
D. Alternating τ_i^z variables	11
E. Bosonization	12
F. Renormalization group analysis	14
V. Many-Body Localization	16
A. Weakly-Coupled Rungs limit	16
B. Heisenberg chain	17
C. Long time evolution	18
VI. Conclusion	19
A. Numerical implementation	20
B. Derivation of Four-Body Hamiltonian	21

I. INTRODUCTION

The study of interacting quantum many-body systems has led to the discovery of a wide variety of phases of matter. A key question is how different phases can be characterized and distinguished from each other, ultimately leading to the question of phase transitions. Understanding the physical phenomena associated to these phases of matter and their transitions emerging due to their many-body nature is important from a fundamental aspect and it is also promising for applications to material science, as well as quantum computation, for example. A central question is about the role of gauge theories associated to symmetries of the system. In spin systems, it is quite natural to identify \mathbb{Z}_2 -symmetries, under which the Hamiltonian remains invariant. Consider for example the classical Ising chain with

$$H = J \sum_j \sigma_j \sigma_{j+1},$$

which is obviously invariant under a simultaneous transformation $\sigma_j \rightarrow -\sigma_j$ on all sites. \mathbb{Z}_2 lattice gauge theories emerge in a variety of strongly-correlated systems such as Ising and Kitaev spin models, high-Tc superconductors and light-matter Hamiltonians [1, 2].

On the other hand, the application of a uniform magnetic field generates a $\mathbb{U}(1)$ gauge field inducing a variety of interesting phases in lattice systems. Examples include a Meissner-like phase, vortex phase or fractional quantum Hall phases [3–6]. Here, we propose a model combining features of both effects: On the one hand, we will map a bosonic ladder model to a quantum spin chain with \mathbb{Z}_2 -symmetry. On the other hand, we will include a $\mathbb{U}(1)$ gauge field which allows us to define a current flow in the system. This current shows characteristics intrinsic to some of the aforementioned phases - for example, we can use it as a manifestation of a Meissner-like phase [3]. In addition, we will try to use it as an indicator for other phenomena, notably to characterize the response of the system to disorder.

Including the effects of impurities is crucial for 'real world' applications, as here one always has to deal with a certain degree of disorder. The inevitability to applications makes it plausible to consider disorder as inherent to the system, which will be the case for the model we consider here. This opens the door to the vast field of research about localization phenomena and disorder effects, which turned out to be not only considerable for many-body physics, but became a whole topic for itself.

The basic question in this area goes back to Anderson, who asked how mobile particles can get localized in the presence of disorder [7]. It turned out that this localization can even occur in the presence of interactions [8–11], leading recently to many-body localization which is an active area of both experimental and theoretical research [12, 13]. Recently, the case of mobile impurities in a quantum fluid has been shown to result in interesting resonance phenomena [14] related to the Kane-Fisher double barrier model [15], which motivates us to study here localization phenomena due to moving impurities forming a telegraph potential. Related to phases of matter and transitions between them, disorder and impurities produce interesting physics which is worth being studied through different probes. In turn, the transition between different types of localization is not fully understood, in particular with respect to many-body localization [16]. One of the most striking characteristics of many-body localized phases is that they do not fulfill the eigenstate thermalization hypothesis, meaning that the initial state will manifest itself in all later states of the system [13, 17, 18]. This property and transitions have been thoroughly analyzed using bipartite fluctuations and entanglement measures [16, 19].

In this article, we will build conclusions about the localization by directly considering the current along a ladder-shaped lattice in the situation where the impurities form the telegraph signal, i.e. impurities correspond to two-state systems occupying either the top or the bottom wire (leg) and forming effectively spin-1/2 degrees of freedom. The current here refers to a Meissner superfluid response for bosonic particles stabilized with a Josephson coupling in the presence of a uniform magnetic field i.e. the $\mathbb{U}(1)$ gauge field. The bosons-impurities coupling produces a direct link towards \mathbb{Z}_2 gauge theories allowing us to study the interplay between the effect of the applied $\mathbb{U}(1)$ and intrinsic \mathbb{Z}_2 gauge fields. We study the correlated limit referring to the rung-Mott phase with one particle per rung such that the superfluid response is a spin-Meissner current [3]. We will also address the persistent current limit when decreasing progressively the strength of the Josephson effect between the wires. We present various analytical methods with numerical exact diagonalizations (ED).

The ladder geometry is frequently being used in cold atom experiments and allows to probe many of the mentioned effects in relation to gauge theories [4, 20, 21]. It has been suggested that it can also be useful to test lo-

calization effects [22–24]. The progress in experimental techniques using Bose-Einstein condensates in optical lattices allows to probe a wide variety of these effects with a high degree of control over the parameters [25, 26]. In these cold atom experiments, both \mathbb{Z}_2 and $\mathbb{U}(1)$ gauge theories can be realized by similar means. Through an appropriate periodic driving protocol, both types of symmetries can be realized on a lattice [21, 27, 28]. A ladder geometry is in this context special as it is quasi-one-dimensional. It allows to test for example one-dimensional physics and is therefore an interesting platform for both experimental and theoretical research.

The article is organized as follows. In Sec. II, we introduce the model and remind definitions related to the rung-Mott state of the bosonic ladder system [3]. In Sec. III, we show distinct limits of solvable quantum dynamics in the presence of impurities associated to a smooth localization of the Meissner superfluid response, with a power-law profile, in the situation of *weakly-coupled rungs*. We will first study the case of static impurities behaving then as purely classical objects commuting with the Hamiltonian and then the case where impurities acquire a quantum dynamics when bouncing back and forth between the top and bottom of the ladder. Four-particle spin Hamiltonians occur in the limit of strong interactions with impurities. In Sec. IV, we describe the limit of *strong inter-rung* interactions applying a rotation on the many-body Hamiltonian. We make a bridge with fermions through the Jordan-Wigner transformation in the case of the telegraph signal when averaging on different configurations showing the occurrence of an insulating phase for the *a*-particles at strong-coupling with the impurities. We also address the specific case of aligned impurities. For the situation of antiferromagnetically aligned impurities, we apply the bosonization formalism of Luttinger liquids [29] and renormalization group arguments. We also observe a strong (steep) localization effect and compare the results with Gaussian disorder [30]. In Sec. V, we discuss the limit of many-body localization from quantum spin chain models [16, 31], including here the particular profile of the telegraph potential. To realize this limit, the ground state evolves as a mixed state produced after a quench when preparing the system in a Néel state. We study the time-dependent profile of entanglement and bipartite fluctuations measures [16, 19]. Furthermore, we will introduce different quantum spin models with two- and four-particles interactions which may have further insight on many-body quantum dynamics.

The Appendices A and B are devoted to details on the numerical ED approach and on the derivation of the four-body Hamiltonian of Sec. IIIC.

II. THE MODEL

We introduce the bosonic two-leg ladder populated by a particle species which we will in the following often call ‘*a*-particles’ [3, 32]. In this model, we want to access a variety of different scenarios, for which we introduce the following parameters: First of all, there should be hopping along the legs of the ladder, which we consider as the *x*-direction, with an amplitude t_x^a . There is also hopping along the rungs of the ladder, in the *y*-direction, with an amplitude t_y^a . Different phases of this model can be controlled by three energy-scales. A chemical potential μ determines the filling of the ladder. Furthermore, we introduce an on-site repulsion potential U_{aa} penalizing two bosonic particles sitting on the same site. Lastly, we also introduce a potential V_\perp causing repulsion for two particles on the same rung. This setup is shown pictorially in Fig. 1.

The effect of a magnetic field can be included through a Peierls substitution following [3]. In a link to cold atom experiments, this can be realized using a large on-site potential and refacilitating the hopping by driving the system periodically in time [27, 28]. Then, we add a second particle species also living on this same ladder and following its own dynamics, while interacting with the *a*-particles, inspired from [21]. We will call this second particle species ‘*gauge particles*’, ‘*f*-particles’ or the

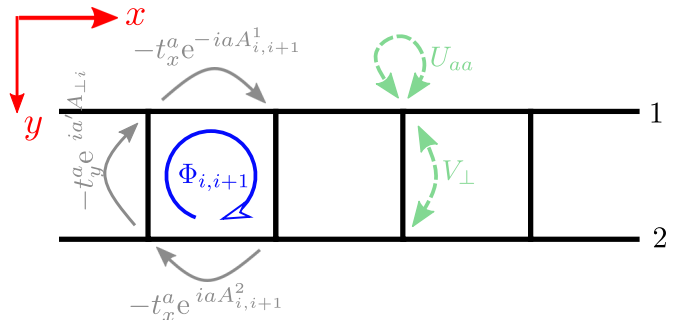


Figure 1: (color online) The setup of a bosonic ladder with hopping strengths (in gray) and potentials felt by the *a*-particles (in green). The effect of a magnetic vector potential enters through the Peierls substitution as complex phases to the hopping strengths. Going around one square plaquette, a flux $\Phi_{i,i+1}$ is acquired.

impurities, where the latter designates the role they are playing in this article. The former is related to the \mathbb{Z}_2 symmetry in the Hamiltonian. A priori, we could imagine a- and f-particles with similar dynamics and influencing each other through an interaction potential. In the following, we will however be mainly interested in the dynamics of the a-particles in the presence of the impurities. We therefore assume to have exactly one f-particle on each rung, which corresponds to half-filling and an infinitely high on-site and on-rung repulsion. The dynamics of the f-particles on the lattice is similar to a telegraphic signal. When these impurities are entirely static, this is similar as imposing a kind of quenched disorder on the a-particles (see Fig. 2).

The interaction between the two particle species is realized in a density dependent way with an energy scale U_{af} . In summary, we get the following Hamiltonian for the a-particles interacting with the impurities:

$$\begin{aligned}
H = & -t_x^a \sum_{\alpha,i} e^{iaA_{i,i+1}^\alpha} a_{\alpha i}^\dagger a_{\alpha,i+1} + \text{h.c.} \\
& -t_y^a \sum_i e^{-ia'A_{\perp i}} a_{2i}^\dagger a_{1i} + \text{h.c.} + \frac{U_{aa}}{2} \sum_{\alpha,i} n_{\alpha i}^a (n_{\alpha i}^a - 1) \\
& + V_\perp \sum_i n_{1i}^a n_{2i}^a - \mu \sum_{\alpha,i} n_{\alpha i}^a + U_{af} \sum_{\alpha,i} n_{\alpha,i}^a n_{\alpha,i}^f. \quad (1)
\end{aligned}$$

We use the following notation: Superscripts a or f designate the respective particle species. In the sums, α denotes the leg of the ladder (1 or 2, as shown in Fig. 1), i goes along the rungs. Consequently, $a_{\alpha i}^\dagger$ and $a_{\alpha i}$ are the bosonic creation and annihilation operators of an a-particle at a rung i and the leg $\alpha = 1, 2$ of the ladder, with the number operator $n_{\alpha i}^a = a_{\alpha i}^\dagger a_{\alpha i}$. The number operator related to the f-particles $n_{\alpha i}^f$ is defined similarly. The phases of the hopping terms enter through a Peierls substitution for a uniform external magnetic field (or gauge field). They are different along the legs ($e^{iaA_{i,i+1}^\alpha}$) and along the rungs ($e^{ia'A_{\perp i}}$) with $A_{i,i+1}^\alpha$ and $A_{\perp i}$ being the

components of the vector potential at the respective link of the ladder and a and a' the respective lattice spacings (see Fig. 1) [3]. The flux per plaquette can be evaluated by a contour integral around a plaquette and through Stokes theorem shows the following relation with a uniform magnetic field [3, 5]:

$$\Phi_{i,i+1} = \oint \mathbf{A} \cdot d\mathbf{l} = -a(A_{i,i+1}^1 - A_{i,i+1}^2) - a'(A_{\perp i+1} - A_{\perp i}). \quad (2)$$

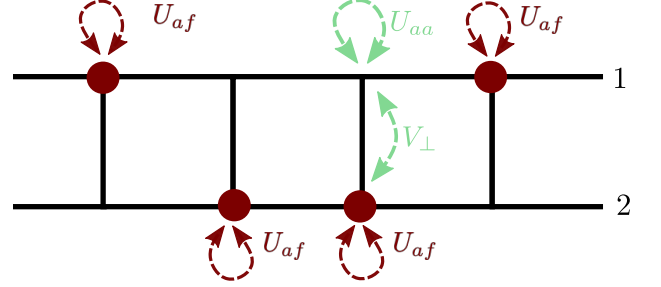


Figure 2: The f-particles shown in red cause an additional on-site potential felt by the a-particles which we call U_{af} . This potential is random in a sense that the f-particles are at each rung randomly placed on one of the two legs referring then to the telegraph signal.

A. Rung-Mott Phase and Definitions

To realize the spin model with the \mathbb{Z}_2 -symmetry, we assume the system to be in the Mott phase for the a-particles. The particles are localized with one particle per rung referring to the rung-Mott state. For clarity's sake, here we fix the definitions starting from Ref. 3. A simple matrix analysis of the system neglecting the interaction with impurities shows that for $t_x^f = 0$, the system is in the Mott phase for $V_\perp + t_y^a > \mu > -t_y^a$. Treating the hopping along the legs of the ladder perturbatively allows to derive the following effective spin Hamiltonian by considering all possible second-order processes:

$$H = \sum_i -2J_{xy} e^{iaA_{i,i+1}^\parallel} \sigma_i^+ \sigma_{i+1}^- + \text{h.c.} + J_z \sigma_i^z \sigma_{i+1}^z - g (\cos(a'A_{\perp,i}) \sigma_i^x - \sin(a'A_{\perp,i}) \sigma_i^y) + \frac{U_{af}}{2} \sigma_i^z \tau_i^z. \quad (3)$$

Here, we define $J_{xy} = (t_x^a)^2/V_\perp$, $J_z = (t_x^a)^2/(2/U_{aa} - 1/V_\perp)$, $g = t_y^a$ and wrote $A_{i,i+1}^\parallel = A_{i,i+1}^1 - A_{i,i+1}^2$. The particle creation and annihilation operators have been replaced by Pauli matrices σ_j and τ_j for effective spins due to a- or f-particles respectively. The second-

order induced terms for the a particles can be identified as a correlated hopping J_{xy} term between the two wires and an Ising J_z interaction term which is tunable when varying the potentials V_\perp and U_{aa} . We have $J_z = 0$ when $V_\perp = U_{aa}/2$. More precisely, we used the

Schwinger-boson representation of the SU(2) algebra [33] with $\sigma_i^x = a_{1i}^\dagger a_{2i} + a_{1i} a_{2i}^\dagger$, $\sigma_i^y = -ia_{1i}^\dagger a_{2i} + ia_{1i} a_{2i}^\dagger$ and $\sigma_i^z = a_{1i}^\dagger a_{1i} - a_{2i}^\dagger a_{2i}$ (and therefore $\sigma_i^+ = a_{1i}^\dagger a_{2i}$ and $\sigma_i^- = a_{1i} a_{2i}^\dagger$). The f-particles are two-state systems which can also be represented similarly through τ Pauli matrices. This is justified since there is precisely one particle of each species on a given rung, as the a-particles are in the Mott phase and we assumed that the f-particles are two-state systems in a general sense e.g. spinless fermions such that $f_{1i}^\dagger f_{1i} + f_{2i}^\dagger f_{2i} = 1$. This allows us to write their states at each rung in the basis $|10\rangle_i, |01\rangle_i$ which can be identified with the spin basis $|\uparrow\rangle_i, |\downarrow\rangle_i$. Without the Peierls phases, the Hamiltonian (3) is that of an XXZ-model in a magnetic field, where the transverse field acting on each rung g represents the Josephson term for the a particles. Here, we also introduce the matter-impurities coupling U_{af} which now represents an Ising coupling between spins. The choice of parameters within the rung-Mott phase for the a particles is motivated by the occurrence a \mathbb{Z}_2 -symmetry under flipping all z-spin components, i.e. changing $\sigma_i^z \rightarrow -\sigma_i^z$ and $\tau_i^z \rightarrow -\tau_i^z$ simultaneously. The term U_{af} can be realized through an interaction between two species similar to a Hubbard interaction.

The local current operator j of a-particles can be evaluated as the time derivative of the particles densities which are related to σ_i^z , as we defined $\sigma_i^z = a_{1i}^\dagger a_{1i} - a_{2i}^\dagger a_{2i} = n_{1i}^a - n_{2i}^a$. This can be computed by $j = -i[H, \sigma_i^z]$ and gives a parallel component j_{\parallel} (proportional to J_{xy}) and a perpendicular component j_{\perp} (proportional to g) [34]

$$j_{\perp} = -2g(\sigma_i^x \sin(a' A_{\perp,i}) + \sigma_i^y \cos(a' A_{\perp,i})), \quad (4a)$$

$$\begin{aligned} j_{\parallel} &= -4iJ_{xy}(e^{iaA_{i,i+1}^{\parallel}} \sigma_i^+ \sigma_{i+1}^- - e^{-iaA_{i,i+1}^{\parallel}} \sigma_i^- \sigma_{i+1}^+), \\ &= 2J_{xy} \left((\sigma_i^x \sigma_{i+1}^x + \sigma_i^y \sigma_{i+1}^y) \sin(aA_{i,i+1}^{\parallel}) \right. \\ &\quad \left. + (\sigma_i^y \sigma_{i+1}^x - \sigma_i^x \sigma_{i+1}^y) \cos(aA_{i,i+1}^{\parallel}) \right). \quad (4b) \end{aligned}$$

Hereafter, we investigate how the parallel current behaves under different configurations of the parameters of this model. In particular, we regard the parallel current for different strengths in the disorder potential U_{af} . In this way, we use it as an indicator for localization and we find different regimes with different localization behaviours. This requires to evaluate the expectation value of the current operator in Eq. (4b) in the ground state of the system by invoking different approximations, which will be explained and justified below. Finally, we compare also to other indicators.

III. WEAKLY-COUPLED RUNG LIMIT

A. Meissner Effect with Static Impurities

The bosonic ladder model introduced in Eq. (1) in its superfluid phase shows an analogue of the Meissner effect [35] through the formation of currents along the legs of the ladder proportional to the negative applied flux and a screening of the currents along the rungs [3, 5]. The existence of a ‘spin-Meissner’-like phase in the Mott-insulating regime seems intuitive at first, and can be understood through the Schwinger-boson representation used to map the model to Eq. (3). In this framework, the magnetic field couples to the spin degrees of freedom [3]. Lattice models with this property can exhibit a spin current even when the charge sector is in an insulating phase [36]. A particle current along one leg is associated to a hole-like current along the other leg. These currents then have a zero net-transfer of charge, and are a manifestation of spin-charge separation [3]. Without impurities, the expectation value of the parallel current operator or simply the parallel current can be evaluated invoking a pinning of the phase due to the dominant g -term as [3]

$$\langle j_{\parallel} \rangle = -2J_{xy} \Phi_{i,i+1}. \quad (5)$$

As for this derivation we require small interactions of a-particles across the rungs we call this limit weakly-coupled rung limit or (almost) decoupled rung limit. We will first study the case of static impurities to show that in the weakly-coupled rung limit, the localization shows a smooth power-law profile as a function of U_{af} , reflecting the classical aspect of the impurities in this situation. Then, as a first situation of mobile quantum impurities, we will study the case of vertical motion described through a transversed field for the τ -spin. This situation precisely refers to the bouncing between top and bottom legs on a given rung such that the effect of impurities can be solved one by one.

Including the effect of impurities and considering g and U_{af} as a magnetic field in transverse and longitudinal direction respectively, the limit is attained if this magnetic field is large compared to J_{xy} and J_z . It is then justified to consider the ground state as the state minimizing the energy on each rung i neglecting the influence of J_{xy} and J_z . We can use a Bloch sphere representation, that

means considering

$$\langle \sigma_i^x \rangle = \sin \Theta_i \cos \rho_i, \quad (6a)$$

$$\langle \sigma_i^y \rangle = \sin \Theta_i \sin \rho_i, \quad (6b)$$

$$\langle \sigma_i^z \rangle = \cos \Theta_i. \quad (6c)$$

Here, Θ_i represents the polar angle and ρ_i the azimuthal angle. Requiring minimization of energy readily yields

$$\rho_i = -a' A_{\perp,j},$$

$$\sin \Theta_i = -\tau_i^z \sin \left(\tan^{-1} \left(-\tau_i^z \frac{2g}{U_{af}} \right) \right) = \frac{2g/U_{af}}{\sqrt{1 + (2g/U_{af})^2}},$$

$$\cos \Theta_i = -\tau_i^z \cos \left(\tan^{-1} \left(-\tau_i^z \frac{2g}{U_{af}} \right) \right) = \frac{-\tau_i^z}{\sqrt{1 + (2g/U_{af})^2}}.$$

From now on, we will assume for simplicity that the phase is the same on each rung and that it furthermore equals the phase for hopping along the legs which we call ϕ . We see that the spin expectation values in this limit on each rung are equal up to a change in τ_i^z . Plugging the obtained results into Eq. (4b) and invoking a mean-field approximation for the two-body terms in the current, we finally obtain

$$\langle j_{\parallel} \rangle = 2J_{xy} \frac{1}{1 + (U_{af}/2g)^2} \sin \phi. \quad (7)$$

This result can be compared to results from ED simulations to show the validity of Eq. (7), which is shown in Fig. 3. In Eq. (7), there is no dependence of the current on a site on the respective τ_i^z -variable. This can be understood since the U_{af} -term gets a second contribution of τ_i^z from the approximate solution for $\langle \sigma_i^z \rangle$, so that we finally have $(\tau_i^z)^2 = 1$ as we are treating these variables as static. In the ED simulations, there is still an influence on the configuration of τ_i^z , since they are performed for small, but non-zero values of J_z and J_{xy} , which is not addressed in the decoupled rung approximation. For that reason, we compare the prediction to the average over all possible configurations of τ_i^z . Throughout this article if not mentioned differently, we indicate expectation values by $\langle \cdot \rangle$, while we denote disorder averages of a quantity A over realizations of τ_i^z disorder configurations by a bar, i.e. \overline{A} . In Fig. 3, we consider the disorder average of the expectation value of the parallel current operator j_{\parallel} , consequently we write $\overline{\langle j_{\parallel} \rangle}$. Details on the numerical implementation can be found in Appendix A. The result (7) shows that the current in this *semiclassical*-impurity regime shows a power-law profile, even for large values of U_{af} in agreement with the numerical results in Fig. 3.

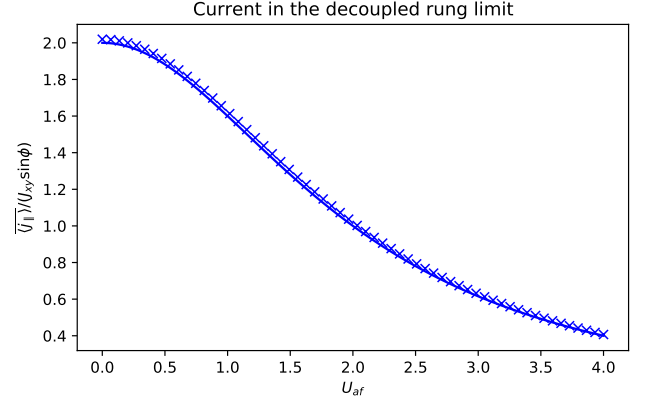


Figure 3: The parallel current $\langle j_{\parallel} \rangle$ as a function of the coupling term U_{af} normalized by $\sin \phi$ and J_{xy} .

Comparison of Eq. (7) (solid line) with simulation results (crosses) obtained as an average over all possible configurations of τ_i^z (we wrote $\overline{\langle j_{\parallel} \rangle}$ in the y-axis to signify that here we are considering a disorder average of the expectation value of the current). The parameters used for this simulation were $J_{xy} = 0.01$, $J_z = 0.01$, $g = 1.0$, $\phi = 0.01$. The simulation was done for a chain with eight sites and periodic boundary conditions. The current was measured between the fourth and the fifth site.

It is also relevant here to distinguish the present situation with the case of one impurity localized at a given site. In the rung-Mott phase the term U_{af} would produce a renormalization of the on-site energy which could be then re-absorbed in the chemical potential μ .

B. Meissner Effect with Mobile Impurities

In the limit of decoupled rungs the f-particles can quite easily be rendered as quantum particles constrained to hopping along a rung, which technically corresponds to addition of a term $-g_f \tau_i^x$ to the Hamiltonian (3). In this case, the impurities behave quantum mechanically and in the formulation of \mathbb{Z}_2 gauge theories [37, 38], the electrical charges ('chargons') associated to τ^x will screen the flux (or 'vison' field) in a unit square $\propto \prod_{l \in \partial p} \tau_l^z$ with ∂p referring to the closed path on a given unit square formed between the two legs, reducing the value of $\langle \tau_l^z \rangle$ on each rung. Note that here the symbol ∂p refers simply to the product of two spin operators in z -direction on successive rungs as the spin variables are defined as delocalized objects on the rungs of the ladder. Below, we study the

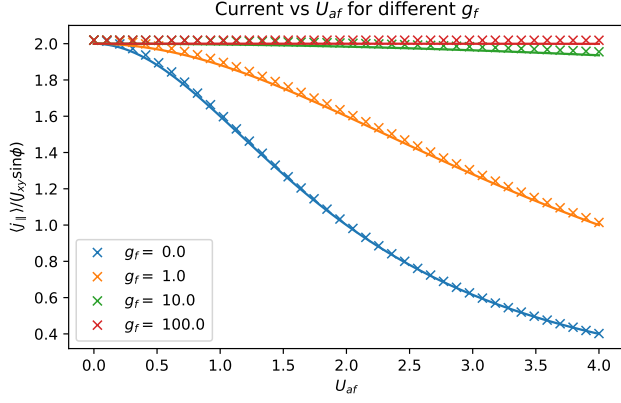


Figure 4: Simulation results (crosses) and predictions from Eq. (8) (solid lines) for the parallel current as a function of U_{af} for different values of g_f in the ground state of the combined system of σ - and τ -spins. For the simulations in this figure, we used $J_{xy} = J_z = 0.01$, $g_a = 1.0$ and $\phi = 0.1$ and a chain with six sites and open boundary conditions. The current was evaluated between the third and the fourth site.

effect of g_f and show that as long as the system remains in the weakly-coupled rungs limit then the localization is smooth with a power-law profile. This then agrees with the fact that \mathbb{Z}_2 gauge fields are effectively ‘screened’.

In the decoupled rung limit with $g, U_{af} \gg J_{xy}, J_z$ the Hamiltonian can then still be diagonalized on each rung and the ground state can be written down, from which expectation values can be evaluated explicitly. Invoking a mean-field approximation for the correlations necessary to compute the parallel current in Eq. (4b), we obtain

$$\langle j_{\parallel} \rangle = 2J_{xy} \frac{1}{1 + \left(\frac{U_{af}/2}{g_a + g_f} \right)^2} \sin \phi. \quad (8)$$

This result can again be verified by comparing to the results from ED simulations which is shown in Fig. 4. As the impurities here are dynamic quantum objects, they do not play the role of a static disorder but rather enter in the evaluation of the ground state through an extension of the Hilbert space of the spin system. Consequently, Fig. 4 does not show an average over disorder configurations, but the expectation value of the parallel current operator in the ground state. For $g_f = 0$, we also verify through Figs. (3) and (4) that the current (density) is identical for periodic and open boundary conditions.

The form of Eq. (8) suggests that the current localizes in a similar fashion as for a static f-particle configuration,

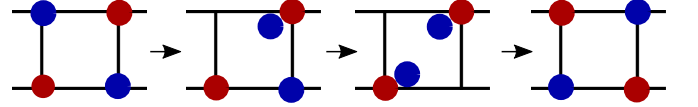


Figure 5: A fourth-order correlated hopping of a- and f-particles, shown with the different colors blue and red respectively, leading to an effective parallel current.

This particular process gives rise to a term $(t_x^a)^2 (t_x^f)^2 / (2(U_{af} + V_{\perp})^3) e^{-ia(A_{i,i+1}^1 - A_{i,i+1}^2)}$.

but a large value of g_f protects the current against the effects of strong coupling between a- and f-particles. In any case, the current in Eq. (8) still follows a power-law profile.

In summary, we have seen that in the decoupled rung limit, which is achieved for weak coupling along the legs of the ladder localization occurs on each rung due to a strong interaction of the a-particle with the f-particle in the form of a power-law, which corresponds to a single-body localization on each rung.

Hereafter, we will now keep the quantum property of the impurities, and in the derivation of an effective spin model from the bosonic model in Eq. (1) turn to the limit where U_{af} is not small compared to U_{aa} and V_{\perp} , but of the same order referring to strong interactions with the impurities.

C. Strong Interactions with Impurities

Here, we will show that when increasing further the interaction strength with impurities, as long as we address the weakly-coupled rungs limit then the sinusoidal response with the $U(1)$ gauge field remains with a power-law form of the prefactor.

When U_{af} is of the same order as U_{aa} and V_{\perp} in Eq. (1) and we allow for hopping of the f-particles in all directions (and not only along the rungs), we have to account for this when doing the perturbation theory. If we consider the Hamiltonian without any hopping and at half filling, the ground state is on each rung two-fold degenerate with one a- and one f-particle on different sites of each rung.

Reintroducing the hopping of a-particles perturbatively again produces second-order Ising interactions such as $J_z^a \sigma_i^z \sigma_{i+1}^z$ with J_z^a different from J_z in the previous sections. Now, introducing a hopping for the impurities (spinless fermions) along both legs and rungs with

$-t_x^f \sum_{\alpha,i} f_{\alpha i}^\dagger f_{\alpha,i+1} - t_y^f \sum_i f_{2i}^\dagger f_{1i} + \text{h.c.}$ with $\alpha = 1, 2$, we get a similar term

$$J_z^f \tau_i^z \tau_{i+1}^z \quad (9)$$

The interchange of an a- and an f-particle along a rung is accounted for by a term

$$-g^{af} e^{ia'A_{\perp,i}} \sigma_i^+ \tau_i^- + \text{h.c.}, \quad (10)$$

where g^{af} is defined differently than g in the previous

sections. Interestingly, the correlated limit with large U_{af} produces a 4-particles correlated hopping term to respect all the interaction terms, as shown exemplarily in Fig. 5. This gives a contribution which reads $-J_{xy}^\parallel e^{ia(A_{\parallel;1}-A_{\parallel;2})} \sigma_i^+ \tau_i^- \sigma_{i+1}^- \tau_{i+1}^+ + \text{h.c.}$

The expressions for the new parameters J_z^a , J_z^f , g^{af} and J_{xy}^\parallel and their derivation can be found in Appendix B for the sake of clarity. We write the effective Hamiltonian as

$$H = -J_{xy}^\parallel \sum_i e^{ia(A_{\parallel;1}-A_{\parallel;2})} \sigma_i^+ \tau_i^- \sigma_{i+1}^- \tau_{i+1}^+ + \text{h.c.} + J_z^a \sum_i \sigma_i^z \sigma_{i+1}^z + J_z^f \sum_i \tau_i^z \tau_{i+1}^z - g^{af} \sum_i e^{ia'A_{\perp,i}} \sigma_i^+ \tau_i^- + \text{h.c.} \quad (11)$$

The parallel current operator can be evaluated from the Hamiltonian as:

$$j_\parallel = -\frac{iJ_{xy}^\parallel}{4} (e^{ia(A_{\parallel;1}-A_{\parallel;2})} (\sigma_i^x \tau_i^x + \sigma_i^y \tau_i^y - i\sigma_i^x \tau_i^y + i\sigma_i^y \tau_i^x) (\sigma_{i+1}^x \tau_{i+1}^x + \sigma_{i+1}^y \tau_{i+1}^y - i\sigma_{i+1}^y \tau_{i+1}^x + i\sigma_{i+1}^x \tau_{i+1}^y) - e^{-ia(A_{\parallel;1}-A_{\parallel;2})} (\sigma_i^x \tau_i^x + \sigma_i^y \tau_i^y + i\sigma_i^x \tau_i^y - i\sigma_i^y \tau_i^x) (\sigma_{i+1}^x \tau_{i+1}^x + \sigma_{i+1}^y \tau_{i+1}^y + i\sigma_{i+1}^y \tau_{i+1}^x - i\sigma_{i+1}^x \tau_{i+1}^y)). \quad (12)$$

When g^{af} is the dominant term, in the ground state we have on each rung

$$\frac{\cos a'A_{\perp,i}}{2} \langle \sigma_i^x \tau_i^x + \sigma_i^y \tau_i^y \rangle + \frac{\sin a'A_{\perp,i}}{2} \langle \sigma_i^x \tau_i^y - \sigma_i^y \tau_i^x \rangle = \frac{1}{2}. \quad (13)$$

This suggests to write

$$\langle \sigma_i^x \tau_i^x + \sigma_i^y \tau_i^y \rangle = 2 \cos a'A_{\perp,i}, \quad (14)$$

$$\langle \sigma_i^x \tau_i^y - \sigma_i^y \tau_i^x \rangle = 2 \sin a'A_{\perp,i}, \quad (15)$$

such that the expectation value of the parallel current reads

$$\langle j_\parallel \rangle = -2J_{xy}^\parallel \sin(\Phi_{i,i+1}). \quad (16)$$

This form agrees with a perfect superfluid in agreement with ED from Fig. 6. In this limit, the interplay between the electric charges and vison fields in the \mathbb{Z}_2 gauge theory produces a renormalization (reduction) of the prefactor J_{xy}^\parallel (see Appendix B). We can compare to the previous result (8) which was derived under the assumption that U_{af} is smaller than U_{aa} and V_\perp . For large U_{af} compared to $g_a + g_f$, we can expand the amplitude of the current expectation value in Eq. (8) to obtain

$$\langle j_\parallel \rangle \propto 8 \frac{(t_x^a)^2 (g_a + g_f)^2}{V_\perp (U_{af})^2}. \quad (17)$$

Using expression (B5) with $t_x^f = 0$ for J_{xy}^\parallel we see that if the hopping amplitudes and the potentials U_{aa} , V_\perp and

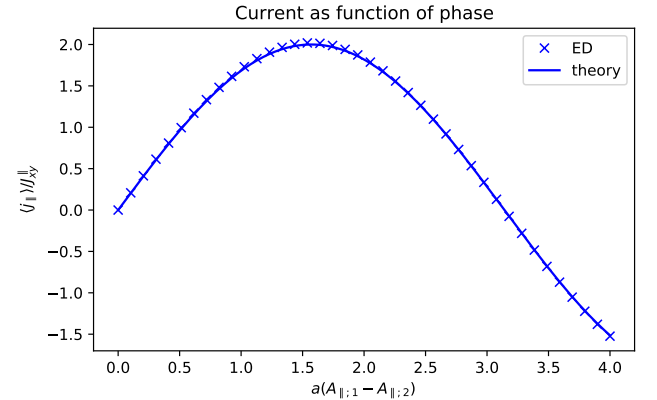


Figure 6: Meissner current in the limit of large U_{af} with the theory from Eq. (16) compared to ED data (crosses) in the ground state of the combined system of σ - and τ -spins. The ED data was obtained for a chain with six sites with periodic boundary conditions. The chosen parameters were $J_{xy}^\parallel = J_z^a = J_z^f = 0.01$, $g^{af} = 1.0$, $a'A_\perp = a(A_{\parallel;1} - A_{\parallel;2})$.

U_{af} are of similar orders of magnitude respectively, both expressions are of a similar form. One important difference of (B5) is however, that the interactions created by the mobility of the impurities are explicitly accounted for.

In the following, we will go back to the model (3) with

static impurities, but consider different cases of strong coupling between the rungs.

IV. STRONGLY-COUPLED RUNGS MODEL

Here, we study the regime of strong inter-rung interactions.

A. Rotation of the Hamiltonian

Starting from the Hamiltonian (3), which was derived under the assumption that $t_x^a, U_{af} \ll U_{aa}, V_\perp$ we proceed by first rotating on each rung around the z-axis using the operator $R_{\phi,i} = \exp\left(-\frac{i\phi}{2}\sigma_i^z\right)$ and consequently rotating around the y-axis using $R_{\Theta,i} = \exp\left(\frac{i\Theta_i}{2}\sigma_i^y\right)$. The angles ϕ and Θ_i are given by the effective mapping of the spin in the decoupled rung limit to the Bloch sphere discussed in the previous subsection (see Eqs. (6)). After this step, the total magnetic field h composed of g and U_{af} points in the z-direction at each rung. If we further invoke that ϕ is small ($\sin \phi \rightarrow 0$) and $U_{af}/2 \gg g$, we obtain to first order in $2g/U_{af}$,

$$H = -J_{xy} \left(\tau_i^z \tau_{i+1}^z \sigma_i^x \sigma_{i+1}^x - \tau_i^z \frac{2g}{U_{af}} \sigma_i^x \sigma_{i+1}^z - \tau_{i+1}^z \frac{2g}{U_{af}} \sigma_i^z \sigma_{i+1}^x + \sigma_i^y \sigma_{i+1}^y \right) \cos \phi \\ + J_z \left(\tau_i^z \tau_{i+1}^z \sigma_i^z \sigma_{i+1}^z + \tau_{i+1}^z \frac{2g}{U_{af}} \sigma_i^x \sigma_{i+1}^z + \tau_i^z \frac{2g}{U_{af}} \sigma_i^z \sigma_{i+1}^x \right) - h \sigma_i^z, \quad (18)$$

with

$$h = g \sin \Theta_i - \frac{U_{af}}{2} \tau_i^z \cos \Theta_i = \frac{2g^2/U_{af} + U_{af}/2}{\sqrt{1 + (2g/U_{af})^2}} \\ = \frac{U_{af}}{2} + \frac{2g^2}{U_{af}} + \mathcal{O}((2g/U_{af})^2). \quad (19)$$

Taking the limit where $J_z = 0$ and $J_{xy} \rightarrow 0$ must be taken with care here. Our results agree with the decoupled-rungs limit of the preceding Section in the sense that for that case the spins are ferromagnetically aligned after the local rotation along the z-direction such that the second-order term J_{xy} becomes effectively inefficient justifying the necessity to take into account the J_{xy}^{\parallel} term in that case to evaluate the current quantitatively.

Below, we will address the cases with a prominent delocalization of a particles along the rungs and also the strong impurities-matter interaction limit. It is relevant to highlight here the occurrence of fourth-order terms occurring both in the correlated dynamics along the wires through the J_{xy} and the interaction term J_z , which trades a non-trivial interplay between the \mathbb{Z}_2 gauge fields and the matter. Therefore, we will address below specific solvable limits which will give us some insight on the physics associated to the model and showing that in the strongly interacting rungs limit, the localization occurs in a steep manner i.e. eventually the current becomes

suppressed at a critical value of U_{af} .

If we consider increasing J_z , while keeping $2g/U_{af} \ll 1$ (so that we can safely neglect terms proportional to $2g/U_{af}$), we see that this term tends to disorder the ferromagnetic order according to the variables τ_i^z and τ_j^z . In this sense, an antiferromagnetic coupling J_z should lead to stronger localization, an observation to which we will address in IV F. On the other hand, if we consider a situation where only h and J_z are relevant to determine the ground state, and we increase U_{af} even further, we will at some point reach the order of magnitude of the potentials ensuring that the f-particles are confined to their initial site. Let us recall that this was one of the basic assumptions we started with: the f-particle configuration is static, so that the τ_i^z -variables are fixed to ± 1 . If we go to U_{af} values so strong that this assumption could be unjustified, then upon increasing J_z , we see that this would favor antiferromagnetic order of the τ_i^z -spins, while h ensures that the σ_i^z -spins are aligned in ferromagnetic order. This is a possibility that was not fulfilled in the derivation of the model (3), so in order to account for it we need to go back to consider the possible hopping processes of the a - and f -particles, as in Sec. III C. In a sense this motivates these aforementioned considerations.

On the other hand, if we neglect g but keep τ_i^z as

static variables, we can consider a transformation of the Hamiltonian (18) by $\sigma_i^x \rightarrow \tau_i^z \sigma_i^x$, $\sigma_i^y \rightarrow \sigma_i^y$ and $\sigma_i^z \rightarrow \tau_i^z \sigma_i^z$ and get an XXZ-model with a random magnetic field with peaked disorder, similarly as when we neglect g directly in the Hamiltonian (3). An investigation of this limit of the model will be the subject of the following Section.

B. The persistent current limit

First, we study the delocalization limit for the a -particles along the rungs where $J_{xy} \gg g$, and for sim-

plicity start with $g = 0$. In this case we can expect a persistent current going along the chain with periodic boundary conditions in the ground state due to the magnetic field which entered through the Peierls substitution into Eq. (3) [39].

If we assume the τ_i^z -variables to be statically fixed to ± 1 and randomly distributed, the model corresponds to a XXZ-chain with a $\mathbb{U}(1)$ gauge field and random magnetic field in z -direction:

$$H = \sum_i \left(-2J_{xy} e^{i\phi} \sigma_i^+ \sigma_{i+1}^- + \text{h.c.} + J_z \sigma_i^z \sigma_{i+1}^z + \frac{U_{af}}{2} \sigma_i^z \tau_i^z \right). \quad (20)$$

This model without the gauge field has been studied in relation with many-body localization and remains an active area of research [12]. Numerically, the model (20) has been considered with $\phi = 0$ and $-J_{xy} = J_z = 0.25$ and a random field of the form $h_i \sigma_i^z$, where h_i are drawn from a uniform distribution [31, 40, 41]. A transition to a many-body localized phase has been found for strong disorder. The same model was used in a recent study suggesting the use of bipartite entanglement and fluctuations to characterize this transition [16]. Here we study the model with a peaked disorder (characterized by $\tau_i^z = \pm 1$) with the energy scale given by U_{af} . We could for example assume that the τ_i^z are at each site independently drawn Bernoulli variables with a universal or site-dependent probability to give ± 1 depending on the physical situation. Considering the σ -spin current between two sites, it varies depending on the configuration of τ -spins on these two sites. This is also confirmed by simulations, as shown in Fig. 8.

The current between two sites depends mainly on whether the τ_i^z -variables on these two sites are equal or opposite. In order to make progress analytically, now we study two limiting cases of configurations, which are in this setup *ferromagnetic* and *antiferromagnetic* order for the impurities and we will compare with the results with those when averaging on various disorder configurations. This will show that owing to a given vison field configuration for the \mathbb{Z}_2 gauge fields the localization indeed occurs in a steep manner. The word steep also refers to an insulating phase for the a -particles, with a zero current.

C. Jordan-Wigner Transformation

Assume that on all rungs, we start with a uniform or ferromagnetic $\tau_i^z = \tau^z = \pm 1$ situation, so that all f -particles live on one leg of the ladder. For $J_z = 0$, the ground state can be found using a mapping to spin-less fermions due to Jordan and Wigner [42]. The Jordan-Wigner transformation

$$\begin{aligned} \sigma_i^+ &\rightarrow c_i^\dagger \exp \left(i\pi \sum_{l<i} n_l \right), \\ \sigma_i^z &\rightarrow 2n_i - 1, \end{aligned} \quad (21)$$

maps the Hamiltonian (3) to

$$H = -2J_{xy} \sum_i e^{i\phi} c_i^\dagger c_{i+1} + \text{h.c.} + \frac{U_{af}}{2} \sum_i (2n_i - 1) \tau_i^z. \quad (22)$$

It can easily be verified that the c_i and c_i^\dagger fulfill fermionic anticommutation relations, which is ensured by the string term $\exp(i\pi \sum_{l<i} n_l)$. Some care needs to be taken about the boundary conditions of the spin chain model: For open boundary conditions, Eq. (22) holds true, but if we want to incorporate periodic boundary conditions, we need to add a term $e^{i\phi} \sigma_N^+ \sigma_1^- + \text{h.c.}$ in the spin chain Hamiltonian (3). After the Jordan-Wigner mapping, it reads

$$\begin{aligned} e^{i\phi} c_N^\dagger e^{i\pi \sum_{l<N} n_l} c_1 + e^{-i\phi} c_1^\dagger e^{-i\pi \sum_{l<N} n_l} c_N \\ = e^{i(\pi(m-1)+\phi)} c_N^\dagger c_1 + \text{h.c.}, \end{aligned} \quad (23)$$

where m denotes the total number of fermions, which is still constant, but according to its parity, we get periodic

or anti-periodic boundary conditions in the free fermion

model. We can then write the full Hamiltonian as

$$H = -2J_{xy} \left[\sum_{i=1}^N e^{i\phi} c_i^\dagger c_{i+1} + \text{h.c.} - (e^{i\pi m} + 1)(e^{i\phi} c_N^\dagger c_1 + \text{h.c.}) \right] + \frac{U_{af}}{2} \sum_i (2n_i - 1) \tau_i^z. \quad (24)$$

We can then go on and diagonalize the Hamiltonian by Fourier transforming separately in the sectors where m is even and odd.

This can be done by introducing Fourier transformed operators:

$$c_j = \frac{1}{\sqrt{N}} \sum_k e^{-ikaj} c_k, \quad (25)$$

with $k = 2\pi n/(Na)$ if m is even and with $k = \frac{2\pi}{a}(\frac{n}{N} - \frac{1}{2})$ if m is odd to account for the anti-periodicity of the boundary conditions, with $n = 0, 1, \dots, N-1$. In the following,

we assume that m is odd and keep in mind that the calculations can easily be generalized to the case where m is even. The Hamiltonian (22) can then upon performing the summation and neglecting a constant term easily be brought to the form

$$H = \sum_k \omega(k) c_k^\dagger c_k \quad (26)$$

with $\omega = -4J_{xy} \cos(ka - \phi) + U_{af} \tau^z$ and a the lattice spacing of the spin chain.

The current calculated from the time derivative takes the form:

$$j_i = 4iJ_{xy} (e^{i\phi} \sigma_i^+ \sigma_{i+1}^- - e^{-i\phi} \sigma_i^- \sigma_{i+1}^+ - e^{i\phi} \sigma_{i-1}^+ \sigma_i^- + e^{-i\phi} \sigma_{i-1}^- \sigma_i^+). \quad (27)$$

The spin current in this basis at a site i is calculated by

$$\begin{aligned} I_i &= -i[H, \sigma_i^z] = -i[H, 2n_i - 1] \\ &= 4iJ_{xy} (e^{i\phi} c_{i-1}^\dagger c_i - e^{i\phi} c_i^\dagger c_{i+1} - \text{h.c.}). \end{aligned} \quad (28)$$

We call the current flowing out from one side j_i , therefore $I_i = j_i - j_{i-1}$ and we can conclude from this and equation (28) that in the ground state (in equilibrium):

$$j = \frac{2}{N} \frac{\partial H}{\partial \phi}. \quad (29)$$

In the ground state, negative energy states will be occupied, i.e.

$$4J_{xy} \cos(ak - \phi) > U_{af} \tau^z,$$

which is fulfilled for k between $k_\pm = \phi/a \pm \arccos\left(\frac{U_{af} \tau_i^z}{4J_{xy}}\right)/a$. This is shown in Fig. 7. The current reads

$$j = \frac{2}{N} \frac{\partial H}{\partial \phi} = -4J_{xy} \frac{2}{N} \sum_k \sin(ak - \phi) c_k^\dagger c_k. \quad (30)$$

For large N , we can write the expectation value of the

current operator as

$$\begin{aligned} \langle j \rangle &= -\frac{4J_{xy}}{\pi} \int_{k_-}^{k_+} dk \sin(ak - \phi) \\ &= \frac{4J_{xy}}{\pi} \cos(ak - \phi) \Big|_{k_-}^{k_+} = 0, \end{aligned} \quad (31)$$

which vanishes in the continuum limit. To explain the

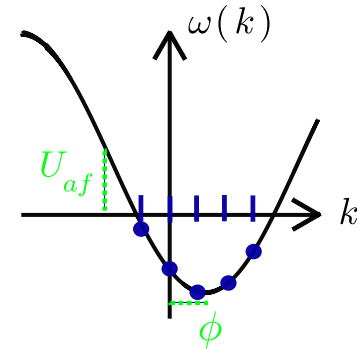


Figure 7: The band is shifted by ϕ/a in k -direction and by U_{af} in the energy, the latter thus has the effect of a chemical potential. The occupied states are shown in blue. The Fermi momenta change accordingly.

current in a finite-size system, we have to stay with the non-continuous case: the allowed momentum values in the first Brillouin zone are $k = 2\pi n/(Na) - \pi/a$ with $n = 0, 1, \dots, N-1$ (or equivalently $2\pi r/L$ with $r = -N/2, -N/2 + 1, \dots, N/2 - 1$), so the momenta are spaced with $2\pi/L$, according to Fig. 7. In order to get a better approximation to the sum in Eq. (30), we can attempt to do the integration as in Eq. (31) exactly between the outermost two occupied states. We therefore

have to change the integration boundaries to

$$\begin{aligned}\tilde{k}_- &= k_- - \Delta_- = k_- - \left(k_- \bmod \frac{2\pi}{L}\right), \\ \tilde{k}_+ &= k_+ - \Delta_+ = k_+ - \left(k_+ \bmod \frac{2\pi}{L}\right).\end{aligned}\quad (32)$$

We obtain the current

$$\langle j \rangle \approx \frac{4J_{xy}}{\pi} \left[\frac{U_{af}\tau_i^z}{4J_{xy}} (-2 \sin \phi \sin \alpha) + \sqrt{1 - \left(\frac{U_{af}\tau_i^z}{4J_{xy}}\right)^2} (2 \sin \phi \cos \alpha) \right], \quad (33)$$

where $\alpha = \arccos\left(\frac{U_{af}\tau_i^z}{4J_{xy}}\right) \bmod \frac{2\pi}{L}$.

Assume L is large, therefore α is small and if furthermore we consider only small phases, the first term becomes negligible and in the second term we can write $\cos \alpha \sim 1$, therefore obtaining

$$\langle j \rangle = 8 \frac{J_{xy}}{\pi} \sqrt{1 - \left(\frac{U_{af}\tau_i^z}{4J_{xy}}\right)^2} \phi. \quad (34)$$

This result can be compared to the results from ED simulations, which can be seen from the solid orange curve in Fig. 8 which shows Eq. (34). The orange crosses show ED results for a setup where on all sites $\tau_i^z = 1$, where we averaged over all sites of the system to make the connection with the calculation in momentum space. Even though in this case, the current has the same sign as in the decoupled rung limit, it is clear by comparing the form of Eq. (7) to Eq. (34) that both regimes are very different, which is also confirmed by simulations. From Fig. 8 (in orange), we see that the simulation results and Eq. (34) agree for the *steep localization* of the current when $U_{af} \sim 4J_{xy}$, i.e. the current now goes to zero. The step-like behavior in ED represented through orange

crosses reflects Fig. 7.

When taking an average over many different realizations of τ_i^z (the blue curve in Fig. 8), this behaviour is changed, but we see that there is still a *strong localization* effect for the same value of U_{af} . It is interesting to observe that the insulating (or localized) regime also occurs in this case.

In order to make more precise statements, we have to consider also other configurations. Precise results can be obtained for the opposite case of alternating τ_i^z -spins, as shown hereafter [43]. We will show that interaction effects through U_{af} favor a strong localization effect similar as in the situation of a Gaussian disorder, as also shown through the green curve of Fig. 8).

D. Alternating τ_i^z variables

First, we address the situation of an alternating or staggered potential and solving the model in the reciprocal space directly. If we set $J_z = 0$ for now, we have

$$H = -2J_{xy} \sum_i e^{i\phi} c_i^\dagger c_{i+1} + \text{h.c.} + U_{af} \sum_i (-1)^i n_i, \quad (35)$$

after a Fourier transform with $x_j = aj$

$$\begin{aligned}H &= -4J_{xy} \sum_k \cos(ak - \phi) c_k^\dagger c_k + U_{af} \sum_j \sum_{k,k'} e^{i(k-k'+\frac{\pi}{a})x_j} c_k^\dagger c_{k'}, \\ &= -4J_{xy} \sum_k \cos(ak - \phi) c_k^\dagger c_k + U_{af} \sum_k c_k^\dagger c_{k+\frac{\pi}{a}},\end{aligned}\quad (36)$$

or in a Bogoliubov-de-Gennes form,

$$H = \sum_{k < 0} (c_k^\dagger \ c_{k+\frac{\pi}{a}}^\dagger) \begin{pmatrix} -4J_{xy} \cos(ak - \phi) & U_{af} \\ U_{af} & -4J_{xy} \cos(ak - \phi + \pi) \end{pmatrix} \begin{pmatrix} c_k \\ c_{k+\frac{\pi}{a}} \end{pmatrix}. \quad (37)$$

This can easily be diagonalized to obtain the eigenenergies

$$E_{\pm} = \pm \sqrt{U_{af}^2 + 16J_{xy}^2 \cos^2(ak - \phi)}. \quad (38)$$

In the ground state, all states giving rise to a negative energy contribution will be occupied in the diagonal basis. The ground state energy is thus

$$E = - \sum_k \sqrt{U_{af}^2 + 16J_{xy}^2 \cos^2(ak - \phi)}. \quad (39)$$

Here the domain of k should have an extension of π/a . Due to the symmetry of the squared-cosine function appearing in Eq. (39), we can sum over any connected region with extension π/a equivalently, in particular we can choose $\phi/a \pm \pi/(2a)$ as summation boundaries which corresponds to those used in Eq. (30) with $U_{af} = 0$. The current can readily be evaluated as a derivative of equation (39) with respect to ϕ and using Eq. (28). It reads

$$j = -\frac{2}{N} \sum_k \frac{16J_{xy}^2 \cos(ak - \phi) \sin(ak - \phi)}{\sqrt{U_{af}^2 + 16J_{xy}^2 \cos^2(ak - \phi)}}. \quad (40)$$

For $U_{af} = 0$, we get back Eq. (30). This result can be compared to the results from ED simulations, which can be seen from the solid green curve in Fig. 8 which shows Eq. (40) for 10 sites. The green crosses show ED results for an alternating configuration $|\uparrow\downarrow\uparrow\downarrow\uparrow\downarrow\uparrow\downarrow\rangle$ of the τ_i^z -spins. To make the connection with the calculation in momentum space leading to Eq. (40), we averaged over all sites of the system.

However, Eq. (40) holds only for $J_z = 0.0$. To depart from this special case, we need to resort to different methods, which we will describe in the following.

E. Bosonization

We now attempt to investigate the special case of disorder treated in the previous Section while including the interaction term proportional to J_z . Our goal is to understand how the sum on momenta evolves in the presence of interactions between fermions mediated by the J_z term here. For this purpose, we will develop a

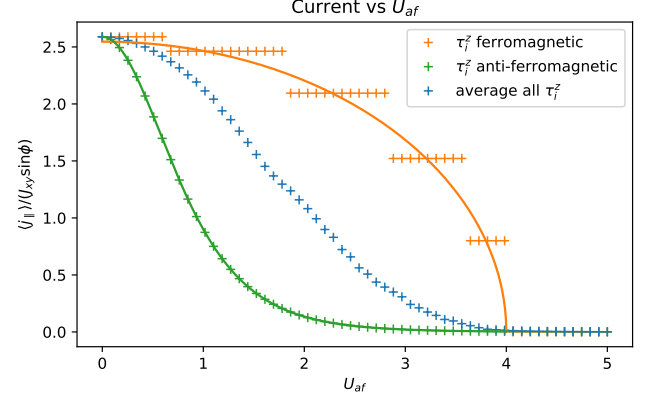


Figure 8: Current averaged over all sites of the system from ED as a function of U_{af} for a ferromagnetically (orange crosses) and an antiferromagnetically (green crosses) ordered configurations of τ_i^z -variables. The blue crosses show an average ($\langle j_{\parallel} \rangle$) over all possible configurations of τ_i^z (here the number of sites $N = 10$, so there are $2^{10} = 1024$ possible configurations). We further used $J_{xy} = 1.0$, $J_z = g = 0.0$, $\phi = 0.01$ and periodic boundary conditions. The analytical formula (34) obtained for a ferromagnetic configuration is the orange solid line, while Eq. (40) is shown by the green solid line.

bosonized theory, which simplifies the understanding of these four-body terms. In the next Section, we will then apply Renormalization Group arguments. To develop this framework, start with the interacting fermion-model

$$H = -2J_{xy} \sum_i c_i^\dagger c_{i+1} + \text{h.c.} + J_z \sum_i (2n_i - 1)(2n_{i+1} - 1) + \frac{U_{af}}{2} \sum_i \tau_i^z (2n_i - 1), \quad (41)$$

which resembles the Hamiltonian (3) in fermionic language with $g = 0$ and without the Peierls phases. For simplicity here, we set the $U(1)$ gauge field $\phi \rightarrow 0$ and we will comment on the effect of ϕ at the end of Sec. IV F.

As we described in Sec. IV C, the Jordan-Wigner transformation maps between spin operators and fermionic operators on a chain. We can identify the spin

raising and lowering operators with creation and annihilation fermion operators

$$c_i^\dagger = s_i^\dagger e^{i\pi \sum_{j<i} n_j}. \quad (42)$$

We can decompose the bosonic operator into a density and a phase [8, 44]:

$$s_i^\dagger = \sqrt{\rho_i} e^{i\tilde{\theta}_i}. \quad (43)$$

If we only consider low energy excitations, we can linearize the spectrum around the Fermi momenta and define left- and right-moving fermions according to the side of the spectrum at which they arise [30]. This corresponds to the description of the free fermion model as a Luttinger liquid [29, 30]. Passing to the continuum limit and using the relations (42) and (43), while changing the sum to an integral over an infinite chain, we can write for the left- and right-moving fermions upon linearizing the spectrum [8, 45]:

$$c_{R/L}^\dagger(x) = \frac{c_{j,R/L}^\dagger}{\sqrt{a}} \approx \frac{1}{\sqrt{a}} e^{i\tilde{\theta}(x)} e^{\pm i\pi \int_{-\infty}^x \rho(x) dx}. \quad (44)$$

We decompose the continuous density operator into a mean and fluctuations $\rho(x) = (\rho_0 + \tilde{\rho})$ with $\rho_0 = ak_F/\pi$. Quantum mechanics imposes the commutation relation $[\tilde{\theta}(x), \tilde{\rho}(y)] = i\delta(x-y)$ between the density and the phase [8]. We can write

$$\rho(x) = \rho_0 + \frac{\partial_x \tilde{\phi}(x)}{\pi}, \quad (45)$$

where we introduced the field $\phi(x)$ by $\tilde{\rho} = \partial_x \tilde{\phi}(x)/\pi$ (we introduce the phase $\tilde{\phi}$ and accordingly $\tilde{\theta}$ to distinguish with the phase ϕ from Eqs. (4)). Then the above commutation relation is achieved for $[\tilde{\theta}(x), \tilde{\phi}(y)] = i\frac{\pi}{2} \text{sgn}(x-y)$. Plugging the form of $\tilde{\rho}$ into Eqs. (44) gives upon accounting for the normalization imposed by Eq. (45)

$$c_R^\dagger(x) = \frac{1}{\sqrt{2\pi a}} e^{i\tilde{\theta}(x)} e^{ik_F x} e^{i\tilde{\phi}}, \quad (46a)$$

$$c_L^\dagger(x) = \frac{1}{\sqrt{2\pi a}} e^{i\tilde{\theta}(x)} e^{-ik_F x} e^{-i\tilde{\phi}}. \quad (46b)$$

In order to retain fermionic commutation relations, we need to multiply the right-hand sides of the equations (46) by the respective Klein factors $U_{R/L}$ where $U_R U_L = i$ [45]. The total density is

$$\rho(x) = \rho_0 + \frac{\partial_x \tilde{\phi}}{\pi} = c_R^\dagger c_R + c_L^\dagger c_L + e^{i2k_F x} c_R^\dagger c_L + e^{-i2k_F x} c_L^\dagger c_R,$$

and we can write the density fluctuations as

$$\frac{\partial_x \tilde{\phi}}{\pi} = \lim_{a \rightarrow 0} c_R^\dagger(x+a) c_R(x) + c_L^\dagger(x-a) c_L(x).$$

Regarding the hopping part of the initial Hamiltonian (41) and going to the continuum limit, we get

$$H = -2J_{xy} \int dx c^\dagger(x) c(x+a) + \text{h.c.}$$

Splitting into the right- and left-moving branches and taking the limit of $a \rightarrow 0$, we obtain after an integration by parts the Hamiltonian in the Dirac-form,

$$H = iv_0 \int dx (c_R^\dagger(x) \nabla c_R(x) - c_L^\dagger(x) \nabla c_L(x)), \quad (47)$$

with $v_0 = 4aJ_{xy}$. The Hamiltonian in terms of the fields $\tilde{\phi}$ and $\tilde{\theta}$ reads

$$H = \frac{v_0}{2\pi} \int dx ((\partial_x \tilde{\theta})^2 + (\partial_x \tilde{\phi})^2). \quad (48)$$

The interaction term in Eq. (41) takes the form $4J_z \sum_i (n_i - \frac{1}{2})(n_{i+1} - \frac{1}{2})$. As we consider the system at half-filling, we can replace terms like $n_i - \frac{1}{2}$ directly by the density fluctuations and then write in the continuum limit and omitting the rapidly oscillating parts:

$$a4J_z \int \left(\frac{\partial_x \tilde{\phi}}{\pi} \right)^2 = \frac{a8J_z/\pi}{2\pi} \int dx (\partial_x \tilde{\phi})^2,$$

so that the interacting Hamiltonian can be written upon introducing the Luttinger parameter K and renormalizing the velocity v as

$$H = \frac{v}{2\pi} \int dx \frac{1}{K} (\partial_x \tilde{\phi})^2 + K (\partial_x \tilde{\theta})^2, \quad (49)$$

with $v/a = \sqrt{(4J_{xy})^2 + 32J_z J_{xy}/\pi}$ and $K = \sqrt{4J_{xy}/(4J_{xy} + 8J_z/\pi)}$.

Now, we include a staggered magnetic field $\frac{U_{af}}{2} \sum_i (-1)^i 2n_i$ to the Hamiltonian. In the continuum limit, this reads

$$\begin{aligned} & \frac{U_{af}}{2a} \int dx (-1)^{x/a} (c_L^\dagger c_L + c_R^\dagger c_R) \\ & + \frac{U_{af}}{2\pi a} \int dx (-1)^{x/a} i e^{i2k_F x} e^{i2\tilde{\phi}} + \text{h.c.} \end{aligned}$$

The first integral can be neglected as it is oscillating rapidly. The second one can be written as

$$-\frac{U_{af}}{\pi a} \int dx \sin(2\tilde{\phi}).$$

Then the full Hamiltonian reads

$$H = \frac{v}{2\pi} \int dx \left(\frac{1}{K} (\partial_x \tilde{\phi})^2 + K (\partial_x \tilde{\theta})^2 \right) - \frac{1}{\pi} \int dx \frac{U_{af}}{a} \sin(2\tilde{\phi}). \quad (50)$$

From Eq. (50), it is evident that if U_{af} is large, the sine-Gordon term dominates and we can anticipate a pinning of ϕ to $\pi/2$, so the system acquires a gap in the energy spectrum. Hereafter, we will look at the opposite case of small U_{af} , such that we can treat the sine-Gordon term as a perturbation. The pinning of the phase $\tilde{\phi}$ also engenders an exponential suppression of the current through the conjugate phase $\tilde{\theta}$.

F. Renormalization group analysis

From now on, we assume that $U_{af} \ll J_{xy}$ so that we can do a perturbative analysis in the matter-impurities interaction. Our objective here is to write down the Renormalization Group (RG) equation for U_{af} using the standard methodology [30]. Assume we change the lattice parameter $a \rightarrow a' = ae^{dl} \approx a(1+dl)$. From this it follows that $dl = \log(a'/a)$. We demand that the partition function remains unchanged under this transformation, i.e. $Z(a') = Z(a)$. Here, this gives the equation:

$$\frac{U_{af}^2(a)}{a^2} a^{2K} = \frac{U_{af}^2(a')}{a'^2} a'^{2K}. \quad (51)$$

It is useful to redefine the dimensionless quantity $g_{af} = U_{af}a/v$ such that

$$g_{af}^2 a^{2K-4} = g_{af}^2(a') a'^{2K-4}.$$

Upon scaling the lattice constant $a' = ae^{dl}$ we obtain

$$\frac{dg_{af}}{dl} = (2-K)g_{af}. \quad (52)$$

Now for the simple case of $J_z = 0$ we have $K = 1$. Therefore, upon increasing l , we also enhance g_{af} . Define $g_{af}(l^*)$, at which this term is for general K of the same order as the hopping term. Solving the differential equation (52) by integrating from a to l we get

$$\frac{g_{af}(l)}{g_{af}(a)} = \left(\frac{a(l)}{a} \right)^{2-K}. \quad (53)$$

We fix l^* at which the impurities-matter term is strongly renormalized and becomes comparable to the kinetic energy, which gives

$$g_{af}(l^*) = \frac{J_{xy}a}{v}, \quad (54)$$

and therefore:

$$l^* \sim a \left(\frac{v}{aU_{af}} \right)^{\frac{1}{2-K}}. \quad (55)$$

In fact, for weak Gaussian disorder, an RG equation similar to (52) can be found following Ref. [30] and reads translated to our setup

$$\frac{dg_{af}}{dl} = (3-2K)g_{af}, \quad (56)$$

leading to an estimation of the localization length

$$l^* \sim a \left(\frac{v}{aU_{af}} \right)^{\frac{1}{3-2K}}. \quad (57)$$

The expressions (55) and (57) quantify the gap opened by a sine-Gordon term, which arises from a staggered magnetic field or a Gaussian disorder in the original model. It is interesting to observe that for $J_z = 0$, the localization lengths of the telegraph potential and of the Gaussian disorder situations are very similar which comforts our conclusion that a well-pronounced localization occurs for various forms of random potentials in the strongly-coupled rungs regime.

For $J_z = 0$ and without disorder, the spectrum can be found in momentum space in a similar fashion as Eq. (26)

$$H = -4J_{xy} \sum_k \cos(ak - \phi) c_k^\dagger c_k, \quad (58)$$

from which the current is easily evaluated as

$$j = \frac{2}{N} \frac{\partial H}{\partial \phi} = -4J_{xy} \frac{2}{N} \sum_k \sin(ak - \phi) c_k^\dagger c_k. \quad (59)$$

In both equations, the sum ranges over accessible momentum states, spaced depending on the boundary conditions (see the discussion in Sec. IV C) up to the Fermi momenta $k_F = \pi/(2a)$. Disorder will open a gap quantified by l^* . We therefore account for its effect by introducing a cut-off of the sum (59) so that it ranges only over momenta with absolute values smaller than $|k_F - (l^*)^{-1}|$. This can be done numerically to obtain a prediction for the behaviour of the current with a staggered magnetic field and the disorder averaged current expectation value. The approximative nature of Eqs. (55) and (57) can be

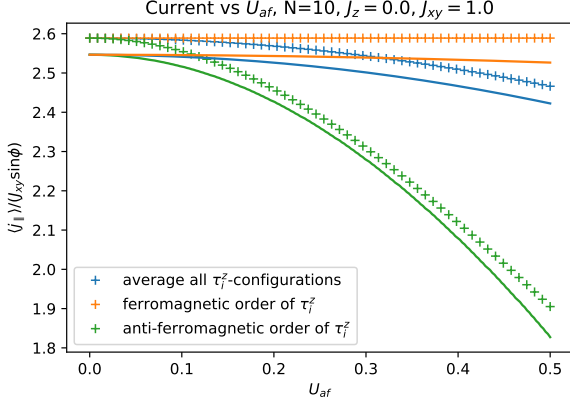


Figure 9: A comparison of results from ED for ferromagnetic, antiferromagnetic and average over all τ_i^z -configurations with $\phi = 0.001$. The theoretical description (34) for a ferromagnetic configuration and the fitting of a truncated sum (59) for the antiferromagnetic and averaged setup respectively are shown as solid lines. To obtain the fit, we sum over 4000 states to obtain a smooth curve. The fitting parameter C in Eq. (60) was evaluated to $C = 0.1624$ for the antiferromagnetic configuration and to $C = 0.3993$ for the average over all disorder configurations. For all three curves, there is an offset which was subtracted during the fitting procedure which is probably due to finite size effects. Here we used a system with $N = 10$ sites and periodic boundary conditions and set $J_{xy} = 1.0$ and $J_z = 0.0$.

accounted for by fitting a free prefactor C , i.e. for $K = 1$ we fit C in

$$l^* = Ca \left(\frac{v}{aU_{af}} \right). \quad (60)$$

In this case, up to this prefactor both cases show the same effects for small U_{af} . This can be confirmed for a small system using numerics, which is shown in Fig. 9. Here, the orange and the green crosses show the current expectation value for a ferromagnetic and an anti-ferromagnetic configuration of the τ_i^z -variables respectively. The blue crosses show an average of the current expectation value over all possible configurations of τ_i^z . Since in Fig. 9 $J_z = 0$, the ED results are the same as in Fig. 8, but with a smaller range of U_{af} . We see that Eq. (40) could account for the full range of U_{af} values in agreement with ED results, while the approach described here holds only for small values of U_{af} . The advantage of the latter is however, that thanks to the bosonized

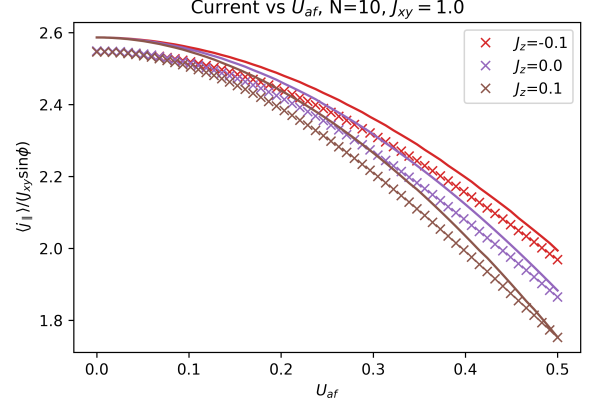


Figure 10: Current from ED as a function of U_{af} with a staggered magnetic field (anti-ferromagnetic configuration of τ_i^z) in comparison to the sum (59) truncated at $|k_F - (l^*)^{-1}|$ (fitted for C). The results are shown for the non-interacting case and for a small positive and negative interaction $J_z = \pm 0.1$. We set $J_{xy} = 1.0$, $g = 0.0$ and $\phi = 0.001$ with periodic boundary conditions. The ED data (crosses) was obtained for a chain with ten sites. The truncated sum (solid lines) was evaluated on a large system with scaled lattice constant in order to get a smooth result (see Appendix A for details) and using a fitting for C .

framework in which we developed it, it is applicable also in the presence of Ising interactions proportional to J_z . We will exploit this in the following.

As we see from Eq. (55), decreasing K (corresponding to an antiferromagnetic coupling $J_z > 0$) leads to a decrease in l^* , therefore the gap increases and there are more terms which are cut off from the sum in equation (59). This effect is stronger than the increase in v coming from an antiferromagnetic coupling J_z , as can be seen from simulation results in Fig. 10. This means that an antiferromagnetic coupling of the σ_i^z -spins in this regime supports the localization of the current, which is seen in Fig. 10 from ED and from the bosonization approach for an antiferromagnetic configuration of the disorder. A ferromagnetic coupling ($J_z < 0$) tends to hinder the localization in this setup, which is in that sense also consistent with the result from the bosonization approach.

To end this section, we remark that for our evaluation of the localization length l^* we assumed for simplicity that $\phi \rightarrow 0$. To include the effects of a finite ϕ perturbatively, one has to add back the Peierls phases to the hopping part of Hamiltonian (41) and rewrite

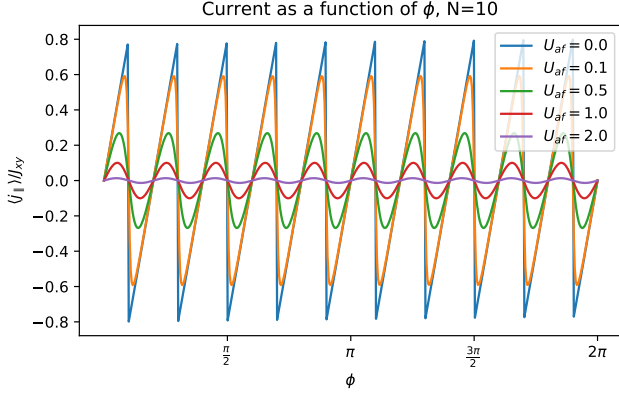


Figure 11: Current for an antiferromagnetic configuration of τ_i^z in a system with $N = 10$ sites, result from ED as a function of ϕ and for a range of U_{af} values. We set $J_{xy} = 1.0$, $J_z = 0.0$ and $g = 0.0$ with periodic boundary conditions.

them in terms of the sine and the cosine of ϕ . Considering only the cosine part, we see that this changes $J_{xy} \rightarrow J_{xy} \cos \phi$, so for small phases one can consider the correction $J_{xy} \rightarrow J_{xy}(1 - \phi^2)$. This would modify both v and K . On a more general note, for the small systems considered and with an antiferromagnetic configuration of the τ_i^z -variables the current depends on ϕ in a periodic way depending on the number of sites. This is shown for $J_z = 0$ in Fig. 11. The ED result presented there agrees with Eq. (40), from which also the dependence of period on the number of available momentum states and thereby on the number of sites can be understood.

In summary, we considered a range of models with strong coupling between the rungs and Ising-type interactions. In the following, we will discuss the possibility of a many-body localized phase for strong disorder.

V. MANY-BODY LOCALIZATION

From Refs. [16] and [40], a disordered potential drawn from a box distribution and $J_z = -J_{xy}$ drives a many-body localized phase. In our case, we are considering a peaked disorder, and therefore it is relevant to study this same limit (implying here $g = 0$). In order to detect a many-body localized phase, we will deviate from the pure ground state by quenching the system from a Néel state and follow the time-evolution of the system. To make a link with the results in Ref. [16], we will study the entanglement entropy and bipartite fluctuations upon

tracing a region of the system [19].

The bipartite fluctuations of the spin in a state $|\psi\rangle$ read [19]

$$\mathcal{F}(l) = \langle \psi | (S_l^z)^2 | \psi \rangle - \langle \psi | S_l^z | \psi \rangle^2, \quad (61)$$

with $S_l^z = \sum_{i=1}^l \frac{1}{2} \sigma_i^z$. In particular, we will consider the bipartite spin fluctuation of the half chain, i.e. $l = L/2$. First, for a comparison we address the situation with the weakly-coupled rungs limit where we can also solve the dynamics.

A. Weakly-Coupled Rungs limit

In the decoupled rung limit with $g \gg J_{xy}, J_z$, in the ground state evaluated as in III A we can readily calculate the bipartite fluctuation in the ground state which reads

$$\mathcal{F}(l) = \frac{l}{4} \frac{1}{1 + (U_{af}/2g)^2}. \quad (62)$$

So up to a prefactor, it is equal to the parallel current and it scales linearly with the subsystem size. This is independent of the disorder configuration since the localization occurs on each rung independently. In Fig. 12, we show the scaling of the bipartite fluctuation with the subsystem size as an average over disorder configurations which we call $\bar{\mathcal{F}}$. In this section, expectation values are implicit through the definition (61) of the bipartite fluctuation.

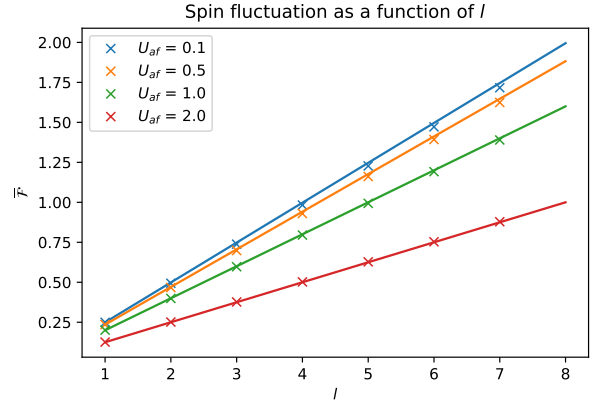


Figure 12: ED results (crosses) in the decoupled rung limit for a range of U_{af} values with $N = 8$, $J_{xy} = J_z = 0.01$, $g = 1.0$, $\phi = 0.01$ and open boundary conditions. The bipartite fluctuation $\bar{\mathcal{F}}$ was evaluated as an average over all possible configurations of τ_i^z . The solid line shows a comparison to Eq. (62). The bipartite fluctuation grows linearly with the subsystem size.

B. Heisenberg chain

In the model of Eq. (3), we can set $J_{xy} = -0.25$, $J_z = 0.25$ and $g = 0$ to make the connection with Ref. [16]. Here, we study the bipartite fluctuations and entanglement measures when tracing half of the system, from the ground state, which will enable us to compare with the situation of a quench studied in the next Section. In the ground state, the bipartite fluctuations can then be evaluated numerically and for a range of J_z we obtain the following results:

The gapless phase of the Heisenberg model is here realized for $-1 < -J_z/J_{xy} \leq 1$ and in that phase, the behaviour is qualitatively the same with a sharp transition to the localized phase for a critical value of disorder strength U_{af} depending on J_z . This can be seen from the curves with the respective values of J_z in Fig. 13, where we plot the average of the bipartite fluctuations over all possible configurations of disorder $\overline{\mathcal{F}}$ against the disorder strength U_{af} . It is interesting to observe that Ising transitions occurring here at $J_z = \pm J_{xy}$ are also clearly visible in Fig. 13.

The scaling of the fluctuations with the subsystem size can be evaluated without disorder and reads [19]

$$\mathcal{F}(l) = \frac{K}{\pi^2} \ln(l) + \frac{f_2}{\pi^2} - A_1 \frac{(-1)^l}{\pi^2 l^{2K}}, \quad (63)$$

where $l = L/2$ refers to the length of one sub-system, i.e. half of the wire, and K is determined from the Bethe

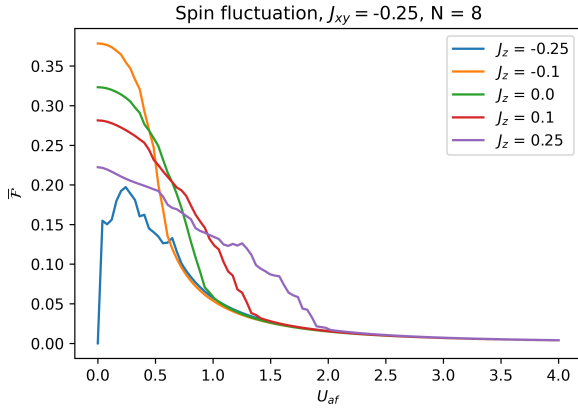


Figure 13: Bipartite fluctuations averaged over all realizations of τ_i^z for $N = 8$ with periodic boundary conditions, the bipartition boundary being in the center of the chain. Here, we set $J_{xy} = -0.25$ and $g = 0.0$, so that the curve with $J_z = 0.25$ bridges with the results in [16]. We furthermore set $\phi = 0.001$.

ansatz solution

$$K = \frac{1}{2} \left(1 - \frac{\cos^{-1} \Delta}{\pi} \right)^{-1}, \quad (64)$$

with $\Delta = -J_z/J_{xy}$. The $\ln l$ behavior comes from a mapping to fermions through the Jordan-Wigner transformation and the A_1 term describes Friedel oscillations of the particle densities from the boundary. Here, the $\ln l$ behavior occurs from gapless modes in the effective fermions theory, and therefore we will refer to this phase at weak-coupling with impurities, i.e., starting from $U_{af} = 0$ as gapless phase.

The scaling (63) of the bipartite fluctuation with subsystem size (for the disorder-free case) should still hold as long as we do not enter the localized phase. This transition can be clearly understood from Fig. 13. In the gapless phase (i.e. at small disorder), interestingly already for small systems sizes, we can fit the parameters f_2 and A_1 in Eq. (63) to the results from the simulation, which is shown in Fig. 14. The simulation results for the gapless phase are here represented by dots, the results from fitting to Eq. (63) are shown by solid lines. The

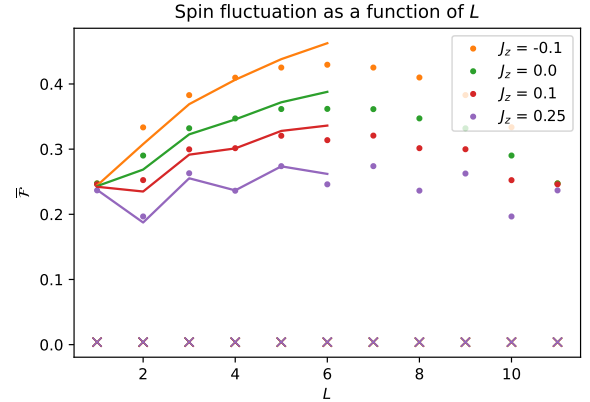


Figure 14: Scaling of the average bipartite fluctuations with the subsystem size for different values of J_z and U_{af} . The dots show simulation results in the gapless phase with $U_{af} = 0.1$. The crosses show results for $U_{af} = 4.0$. Different values of J_z are represented by different colors. The bipartite fluctuation was evaluated for 1000 randomly chosen configurations of τ_i^z and consequently averaged over. These simulations were performed for a chain with 12 sites and periodic boundary conditions. We set $J_{xy} = -0.25$, $g = 0.0$ and $\phi = 0.001$. For the results in the gapless phase (dots), we fit equation (63), the results are represented by solid lines.

results are shown in the Table.

J_z	-0.1	0.0	0.1	0.25
f_2	2.14	2.05	1.93	1.78
A_1	0.27	0.35	0.47	0.56

In the strongly localized regime, the bipartite fluctuation is expected to vanish for any size of the subsystem, which can be confirmed from simulation results shown in Fig. 14, where results for a large value of disorder U_{af} lead to a vanishing bipartite fluctuation for all values of J_z (represented by crosses in the figure).

The entanglement entropy S between two subsystems is defined from the von Neumann entropy by

$$S = -\text{Tr} \rho_A \ln \rho_A, \quad (65)$$

where $\rho_A = \text{Tr}_B(|\psi\rangle\langle\psi|)$ is the density matrix of the ground state with the degrees of freedom of the composite subsystem traced out. We have verified that the entanglement entropy shows a similar transition as the bipartite fluctuations in Fig. 13 (not shown).

C. Long time evolution

We now depart from the analysis of the ground state physics and turn towards a time-dependent description. If we prepare the system of a -particles in the Néel state $|\uparrow\downarrow\uparrow\downarrow \dots \uparrow\downarrow\rangle$ and evolve in time with the Hamiltonian (3) with $J_{xy} = -0.25$, $J_z = 0.25$, $g = 0$ and $\phi = 0.01$, we can evaluate the bipartite fluctuations and the entanglement entropy as an average over all configurations of disorder. We can then qualitatively compare to the results obtained in [16]. We show the results for the bipartite fluctuation in the localized phase (with $U_{af} = 10.0$) in Fig. 15 and for the entanglement entropy in Fig. 16. There we considered the time-evolved state starting from the Néel state for all possible configurations of disorder, evaluated the bipartite fluctuation and the entanglement and consequently averaged over all possible configurations of the disorder. We consequently call the evaluated quantities $\overline{\mathcal{F}}$ and \overline{S} respectively.

We observe a similar behaviour as with a box disorder in Ref. [16]: Both the bipartite fluctuations and the entanglement entropy show a rapid growth at short times, after which the bipartite fluctuations saturate and the entanglement entropy shows a logarithmic growth with time at strong interactions, in agreement with a MBL. The evolution after a long time shows the localization with disorder in Figs. 17 and 18, which is then different

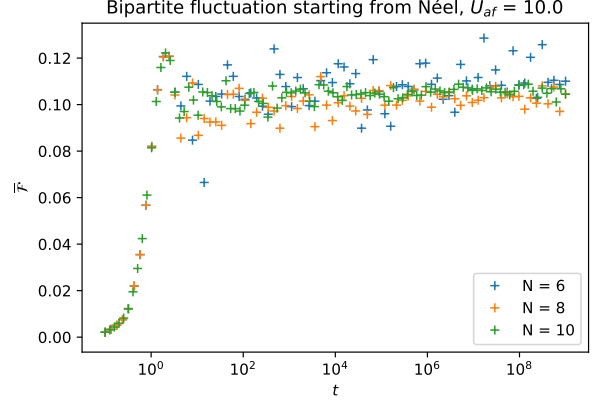


Figure 15: Bipartite fluctuations for $U_{af} = 10.0$, in the localized phase, average over all possible configurations of disorder (for number of sites N , there are 2^N possibilities) with open boundary conditions. Here we set $J_{xy} = -0.25$, $J_z = 0.25$, $g = 0.0$ and $\phi = 0.01$.

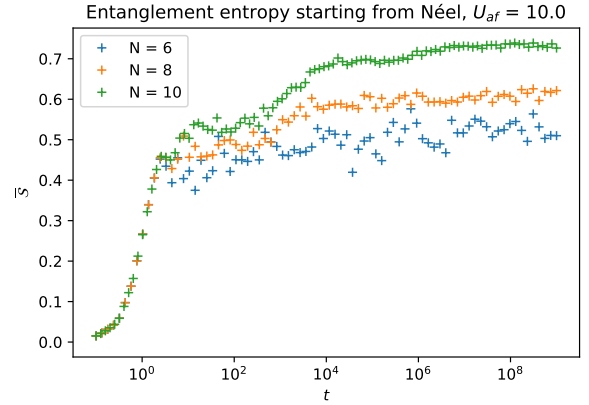


Figure 16: Entanglement entropy for $U_{af} = 10.0$, in the localized phase, average over all possible configurations of disorder with open boundary conditions. Here we set $J_{xy} = -0.25$, $J_z = 0.25$, $g = 0.0$ and $\phi = 0.01$.

than the strongly-localized regime when tracing half of the system from the ground state. In these figures, we show the result for all possible configurations of disorder as a distribution in order to facilitate a comparison with the results obtained in Ref. [16]. The color of a small square inside the plot signifies the absolute number of disorder configurations leading to such a result for the bipartite fluctuation and the entanglement entropy, respectively. The averages over all disorder configurations $\overline{\mathcal{F}}$ and \overline{S} are shown by green dots.

We see that even though for the two special cases of ferro- and antiferromagnetically ordered impurities the

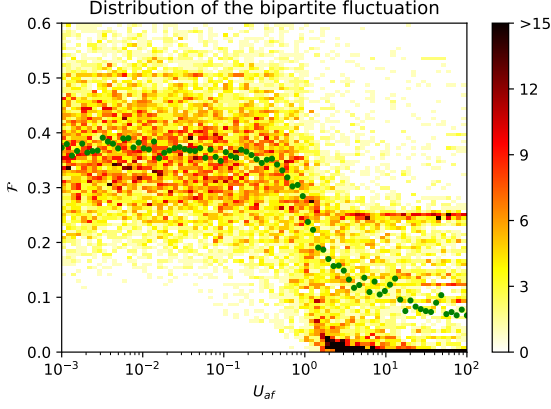


Figure 17: Distribution of the bipartite fluctuations vs U_{af} for $J_{xy} = -0.25$, $J_z = 0.25$, $g = 0$ and $N = 8$ after $t = 10^{16}$. We sampled over all $2^8 = 256$ possible configurations of the τ_i^z -variables. The color scheme shows the absolute number of disorder configurations leading to a result in the respective range. The average \bar{F} over all disorder configurations is shown by green dots.

localization behaviour of the current is fundamentally different, the average of the current over all possible configurations clearly shows different reactions to low and high values of U_{af} . The limit of U_{af} of the same and larger order as J_{xy} and J_z seems most promising to identify a many-body localized phase, but is clearly also difficult to address analytically and needs further investigations in particular to understand the properties of the localized phase.

VI. CONCLUSION

In this article, we have studied a bosonic ladder system populated by two different types of particles and analyzed its response to an applied magnetic field forming a $\mathbb{U}(1)$ gauge field. We considered one particle species as impurities (*f-particles*) and analyzed the effects of their dynamics or disorder on the other particle species (*a-particles*). The impurities are described as two-state systems, e.g. as spinless fermions with a total density one per rung, forming a telegraph potential. In the Mott phase with one delocalized *a*-particle per rung, this model can be mapped to an effective spin model with two different types of spin- $\frac{1}{2}$ operators (σ - and τ -spins). We assumed a density dependent coupling between *a*- and *f*-particles which gave rise to a two-spin operator $\sigma_i^z \tau_i^z$.

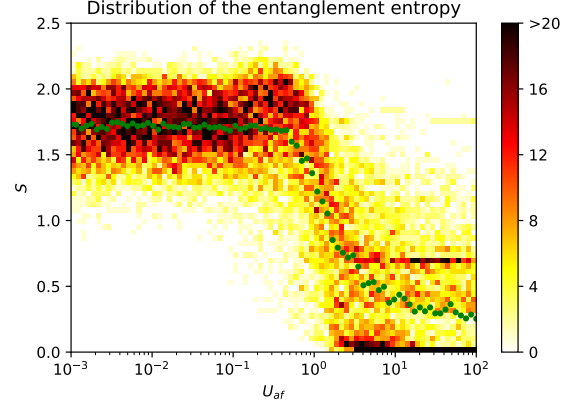


Figure 18: Distribution of the entanglement entropy vs U_{af} for $J_{xy} = -0.25$, $J_z = 0.25$, $g = 0$ and $N = 8$ after $t = 10^{16}$. We sampled over all $2^8 = 256$ possible configurations of the τ_i^z -variables. The color scheme shows the absolute number of disorder configurations leading to a result in the respective range. The average \bar{S} over all disorder configurations is shown by green dots.

The model is invariant after a flip of all *z*-spin components σ_i^z and τ_i^z (\mathbb{Z}_2 -symmetry). We have identified two distinct profiles of localization from the spin-superfluid response of the *a* particles, i.e. a power-law form in the weakly-coupled rung limit and a steep localization (or insulating) behaviour for strongly-coupled rungs where the current becomes strongly suppressed at a critical value of the impurities-matter coupling, and tested various forms of disorder configurations. We have formulated analytical and numerical arguments to justify these conclusions and for the strongly-coupled rung situation we have shown that the steep localization occurring e.g. in the antiferromagnetic case is similar to the case of fermions with a Gaussian disorder potential. For other forms of disorder configurations, the localization profile is distinct but we observe that in all studied cases the current goes to zero for the same critical value of the impurities-matter coupling which then justifies the word steep localization for all these cases assuming the strongly-coupled rungs limit. Finally, we have addressed the many-body localization limit for the present situation of a telegraph signal formed by the impurities when deviating from a pure ground state, applying a quench and following the time evolution from a Néel state in the strong-interaction limit.

Our work opens further perspectives on the role of

multi-particles couplings, gauge theories and many-body localization which can be tested with current quantum technology [20, 46].

Acknowledgements: We acknowledge fruitful discussions with Monika Aidelsburger, Fabian Alet, Camille Aron, Valentina Ros, Thomas Baker, Fabian Grusdt, Nicolas Laflorencie, Alexandru Petrescu, Frank Pollmann and Nicolas Regnault. This work was funded by the Deutsche Forschungsgemeinschaft (DFG, German Research Foundation) under Project No. 277974659 via Research Unit FOR 2414 (including the PhD thesis of EB and FY). FY recently moved to Stockholm University and acknowledges funding from the Swedish Research Council (VR) and the Knut and Alice Wallenberg Foundation. This work has also benefitted from the Hopper cluster at CPhT.

Appendix A: Numerical implementation

The effective spin Hamiltonians (3), (20) and (11) were implemented numerically using the QuTip package for Python [47]. In the case of a static f -particle configuration, the Hilbert space for a chain of length L is 2^L -dimensional and the operators constituting the Hamiltonian are realized by their actual form in this Hilbert space,

$$\sigma_i^+ \sigma_{i+1}^- = \mathbb{1}_1 \otimes \dots \otimes \mathbb{1}_{i-1} \otimes \sigma_i^+ \otimes \sigma_{i+1}^- \otimes \mathbb{1}_{i+2} \otimes \dots \otimes \mathbb{1}_L.$$

In this framework, it is simple to implement the f -particle dynamics using quantum spins as well, in order to check Eq. (8) or to explore the model (11) featuring a four-body interaction. The Hilbert space for a chain of length L is then 2^{2L} -dimensional and the operators take the following form

$$\sigma_i^z \tau_i^z = \mathbb{1}_{\sigma,1} \otimes \mathbb{1}_{\tau,1} \otimes \dots \otimes \mathbb{1}_{\sigma,i-1} \otimes \mathbb{1}_{\tau,i-1} \otimes \sigma_i^z \otimes \tau_i^z \otimes \mathbb{1}_{\sigma,i+1} \otimes \mathbb{1}_{\tau,i+1} \otimes \dots \otimes \mathbb{1}_{\sigma,L} \otimes \mathbb{1}_{\tau,L}.$$

In the implemented program, once the Hamiltonian is defined, the ground state is evaluated numerically. We evaluate the expectation values of the currents by evaluating the expectation values of the spin operators and correlations in Eq. (4).

For certain specialized setups, we can diagonalize the Hamiltonian in momentum space after mapping to free fermions and hence evaluate the current as a sum over occupied momentum states (see Eqs. (30), (40) and (59)). In these cases, the current can be evaluated directly by evaluating occupied momenta (respecting the discretization and boundary conditions, see Sec. IV C) and summing numerically. This procedure has then also been used to evaluate the current in the interacting case with a staggered magnetic field after bosonization. In this case, the sum was truncated to account for the gap opened by the staggered field. Note that due to the numerical simplicity of this approach, significantly larger systems can be analyzed than with the ED approach. The downside is of course that it can only be applied if a mapping to the momentum space is at all possible.

In Sec. IV F, we described how the sum over momentum space can be truncated in order to account for the localization with increasing disorder strength. In Eq. (60), we introduced a fitting parameter C which we evaluated

numerically to make the connection between data from ED and the truncation of the sum in momentum space. The results of this procedure can be seen in Figs. 9 and 10. For the evaluation of the truncated sum in momentum space, we used a large system to approach the continuum limit, necessary for our RG analysis to hold. The ED data can be obtained only for small systems. When comparing the currents without the disorder, there is a small offset between both results which is getting larger for smaller systems in ED. In order to fit C in the localization length, we neglect this offset (i.e. shift both curves onto each other). For the fitting, we use a least square optimizer for the desired range of disorder strength to evaluate C .

In Sec. V, we investigate bipartite spin fluctuations and entanglement entropy. We firstly consider both quantities in the ground state. For that, we evaluate the ground state for each possible configuration of disorder at a certain disorder strength, evaluate the bipartite fluctuation (61) and the entanglement entropy (65) by taking expectation values for each disorder configuration and finally averaged over disorder configurations. When we study the long time evolution in Sec. V C, we prepare the system initially in the Néel state (for the a -particles) and in a certain configuration of disorder. We consider

the evolved state after a time t using the (time) evolution operator expressed as a matrix exponential as

$$|\Psi(t)\rangle = e^{-iH_{\text{dis}}t} |\Psi(0)\rangle. \quad (\text{A1})$$

Here, we wrote H_{dis} to underline the static disorder in the τ_i^z -variables in the Hamiltonian. We then evaluate the bipartite fluctuation (61) and the entanglement entropy (65) using $|\Psi(t)\rangle$. Finally, we average over all disorder

configurations.

Appendix B: Derivation of Four-Body Hamiltonian

As described in Sec. IIIC, if we include hopping of the impurities in all directions, we have to enhance Hamiltonian (1) by these new processes and potentials constraining this mobility. We therefore consider the following Hamiltonian:

$$\begin{aligned} H = & -t_x^a \sum_{\alpha,i} e^{iaA_{i,i+1}^\alpha} a_{\alpha,i}^\dagger a_{\alpha,i+1} + \text{h.c.} - t_y^a \sum_i e^{-ia'A_{\perp,i}} a_{2i}^\dagger a_{1i} - t_x^f \sum_{\alpha,i} f_{\alpha,i}^\dagger f_{\alpha,i+1} - t_y^f \sum_i f_{2i}^\dagger f_{1i} + \text{h.c.} \\ & + \frac{U_{aa}}{2} \sum_{\alpha,i} n_{\alpha,i}^a (n_{\alpha,i}^a - 1) + \frac{U_{ff}}{2} \sum_{\alpha,i} n_{\alpha,i}^f (n_{\alpha,i}^f - 1) + V_\perp \sum_i (n_{1i}^a n_{2i}^a + n_{1i}^f n_{2i}^f) - \mu \sum_{\alpha,i} n_{\alpha,i}^a + U_{af} \sum_{\alpha,i} n_{\alpha,i}^a n_{\alpha,i}^f. \end{aligned} \quad (\text{B1})$$

With respect to the setup (1) where the impurities were considered as static, we added the hopping of the f-particles in x- and y-direction with the amplitudes t_x^f and t_y^f respectively. Furthermore, we added potentials penalising two f-particles sitting on the same site (U_{ff}) and on the same rung (V_\perp) in completely analogous to the a-particle dynamics in Sec. II. While the on-site repulsion (U_{ff}) can be chosen freely, we constrain V_\perp for simplicity to be the same for both a- and f-particles. In the following, we will consider only the limit where formally $U_{ff} \rightarrow \infty$ is the biggest parameter and therefore two impurities cannot occupy the same site. They thus behave like spinless fermions. As in Sec. II, we aim to derive an effective spin model at half-filling of both particle species while now considering U_{af} of the same order as U_{aa} and V_\perp and much larger than the hopping amplitudes. The ground state without hopping is now that with an a- and an f-particle on opposite legs on each rung, there is a \mathbb{Z}_2 gauge freedom on each rung. Restoring the hopping along the legs perturbatively, it gives rise to second order processes for both a- and f-particles in an analogous way as in Sec. II which can be written as

$$J_z^a \sigma_i^z \sigma_{i+1}^z + J_z^f \tau_i^z \tau_{i+1}^z \quad (\text{B2})$$

with

$$\begin{aligned} J_z^a &= (t_x^a)^2 \left(\frac{2}{U_{aa}} - \frac{1}{V_\perp + U_{af}} \right), \\ J_z^f &= -\frac{(t_x^f)^2}{V_\perp + U_{af}}. \end{aligned}$$

Due to the mobility of the impurities and the large inter-species interaction U_{af} , the hopping along the rungs also enters through a second order process which accounts for exchange of the two species along a rung which reads

$$-g^{af} e^{ia'A_{\perp,i}} \sigma_i^+ \tau_i^- + \text{h.c.} \quad (\text{B3})$$

with

$$g^{af} = 2 \frac{t_y^a t_y^f}{U_{af}}.$$

To evaluate the current along the legs, processes need to be considered which interchange the a-particle states between two neighboring rungs. Due to the large inter-species potential U_{af} , these interchange also the states of the f-particles so that the relevant processes interchange completely the state between two rungs. Such processes arise to fourth order in perturbation theory for neighbouring rungs with initially different configuration. Therefore, all of the resulting terms contain either the four-body operator $\sigma_i^- \tau_i^+ \sigma_{i+1}^+ \tau_{i+1}^-$ or its Hermitian conjugate. We can distinguish such processes where the a-particles hop only along the legs (one of them is shown exemplarily in Fig. 5) which bear a phase factor $e^{ia(A_{\parallel;1} - A_{\parallel;2})}$ or its Hermitian conjugate, and such processes where the a-particles hop only along the rungs, therefore having a phase factor $e^{ia'(A_{\perp;i} - A_{\perp;j})}$ or its Hermitian conjugate. Note that we consider a setup where the f-particles are not affected by the magnetic field and therefore do not acquire a phase upon hopping. Altogether and with our

assumptions we can identify 88 fourth order processes leading to an exchange of two initially different configu-

rations between neighbouring rungs on a plaquette. We can write the arising term as

$$- (J_{xy}^{\parallel} e^{-ia(A_{\parallel;1}-A_{\parallel;2})} + J_{xy}^{\perp} e^{-ia'(A_{\perp;i}-A_{\perp;i+1})}) \sigma_i^- \tau_i^+ \sigma_{i+1}^+ \tau_{i+1}^- + \text{h.c.}, \quad (\text{B4})$$

with

$$J_{xy}^{\parallel} = \frac{8(t_x^a)^2(t_y^f)^2}{U_{af} + V_{\perp}} \left(\frac{1}{U_{af}^2} + \frac{1}{U_{af}(U_{af} + V_{\perp})} + \frac{1}{2(U_{af} + V_{\perp})^2} \right) + \frac{8(t_x^a)^2(t_x^f)^2}{(U_{af} + V_{\perp})^2} \left(\frac{1}{2U_{af}} + \frac{1}{2V_{\perp}} + \frac{1}{2U_{af} + 2V_{\perp}} \right), \quad (\text{B5})$$

$$J_{xy}^{\perp} = 8 \frac{(t_y^a)^2(t_y^f)^2}{U_{af}^3} + 8 \frac{(t_y^a)^2(t_x^f)^2}{U_{af} + V_{\perp}} \left(\frac{1}{U_{af}^2} + \frac{1}{U_{af}(U_{af} + V_{\perp})} + \frac{1}{2(U_{af} + V_{\perp})^2} \right). \quad (\text{B6})$$

$$(\text{B7})$$

As we are mainly interested in the parallel current and we assume that the term (B3) is dominant, the terms proportional to J_{xy}^{\perp} in (B8) can be neglected as in that case as the total phase vanishes there. We therefore consider

only the term

$$- J_{xy}^{\parallel} e^{-ia(A_{\parallel;1}-A_{\parallel;2})} \sigma_i^- \tau_i^+ \sigma_{i+1}^+ \tau_{i+1}^- + \text{h.c.} \quad (\text{B8})$$

-
- [1] X.-G. Wen, *Quantum field theory of many-body systems: from the origin of sound to an origin of light and electrons*. Oxford University Press on Demand, 2004.
 - [2] S. Sachdev, *Quantum Phase Transitions*. Cambridge University Press, 2 ed., 2011.
 - [3] A. Petrescu and K. Le Hur, “Bosonic Mott insulator with Meissner currents,” *Physical review letters*, vol. 111, no. 15, p. 150601, 2013.
 - [4] M. Atala, M. Aidelsburger, M. Lohse, J. T. Barreiro, B. Paredes, and I. Bloch, “Observation of chiral currents with ultracold atoms in bosonic ladders,” *Nature Physics*, vol. 10, no. 8, p. 588, 2014.
 - [5] E. Orignac and T. Giamarchi, “Meissner effect in a bosonic ladder,” *Physical Review B*, vol. 64, no. 14, p. 144515, 2001.
 - [6] K. Le Hur, L. Henriet, L. Herviou, K. Plekhanov, A. Petrescu, T. Goren, M. Schiro, C. Mora, and P. P. Orth, “Driven dissipative dynamics and topology of quantum impurity systems,” *Comptes Rendus Physique*, vol. 19, no. 6, pp. 451–483, 2018.
 - [7] P. W. Anderson, “Absence of diffusion in certain random lattices,” *Physical review*, vol. 109, no. 5, p. 1492, 1958.
 - [8] M. P. Fisher, P. B. Weichman, G. Grinstein, and D. S. Fisher, “Boson localization and the superfluid-insulator transition,” *Physical Review B*, vol. 40, no. 1, p. 546, 1989.
 - [9] T. Giamarchi and H. J. Schulz, “Anderson localization and interactions in one-dimensional metals,” *Physical Review B*, vol. 37, p. 325, 1988.
 - [10] G. Lemarié, I. Maccari, and C. Castellani, “Kane-fisher weak link physics in the clean scratched-xy model,” *Physical Review B*, vol. 99, p. 054519, 2019.
 - [11] E. V. H. Doggen, G. Lemarié, S. Capponi, and N. Laflorencie, “Weak versus strong disorder superfluid-bose glass transition in one dimension,” *Physical Review B*, vol. 96, p. 180202, 2017.
 - [12] F. Alet and N. Laflorencie, “Many-body localization: An introduction and selected topics,” *Comptes Rendus Physique*, vol. 19, no. 6, pp. 498–525, 2018.
 - [13] D. A. Abanin, E. Altman, I. Bloch, and M. Serbyn, “Colloquium: Many-body localization, thermalization, and entanglement,” *Reviews of Modern Physics*, vol. 91, no. 2, p. 021001, 2019.
 - [14] T. L. Schmidt, G. Dolcetto, C. J. Pedder, K. Le Hur, and P. P. Orth, “Mechanical resonances of mobile impurities in a one-dimensional quantum fluid,” *Phys. Rev. Lett.*, vol. 123, p. 075302, 2019.
 - [15] C. L. Kane and M. P. A. Fisher, “Transmission through barriers and resonant tunneling in an interacting one-dimensional electron gas,” *Phys. Rev. B*, vol. 46, p. 15233, 1992.
 - [16] R. Singh, J. H. Bardarson, and F. Pollmann, “Signatures of the many-body localization transition in the dynamics of entanglement and bipartite fluctuations,” *New Journal*

- of Physics*, vol. 18, no. 2, p. 023046, 2016.
- [17] M. Rigol, V. Dunjko, and M. Olshanii, “Thermalization and its mechanism for generic isolated quantum systems,” *Nature*, vol. 452, no. 7189, pp. 854–858, 2008.
 - [18] D. A. Huse, R. Nandkishore, V. Oganesyan, A. Pal, and S. L. Sondhi, “Localization-protected quantum order,” *Physical Review B*, vol. 88, no. 1, p. 014206, 2013.
 - [19] H. F. Song, S. Rachel, C. Flindt, I. Klich, N. Laflorencie, and K. Le Hur, “Bipartite fluctuations as a probe of many-body entanglement,” *Physical Review B*, vol. 85, no. 3, p. 035409, 2012.
 - [20] C. Schweizer, F. Grusdt, M. Berngruber, L. Barbiero, E. Demler, N. Goldman, I. Bloch, and M. Aidelsburger, “Floquet approach to \mathbb{Z}_2 lattice gauge theories with ultracold atoms in optical lattices,” *Nature Physics*, vol. 15, pp. 1168–1173, 2019.
 - [21] L. Barbiero, C. Schweizer, M. Aidelsburger, E. Demler, N. Goldman, and F. Grusdt, “Coupling ultracold matter to dynamical gauge fields in optical lattices: From flux-attachment to \mathbb{Z}_2 lattice gauge theories,” *Science*, no. 5, p. p. Eaav7444, 2019.
 - [22] F. Crépín, N. Laflorencie, G. Roux, and P. Simon, “Phase diagram of hard-core bosons on clean and disordered two-leg ladders: Mott insulator–luttinger liquid–bose glass,” *Physical Review B*, vol. 84, no. 5, p. 054517, 2011.
 - [23] Y. Ye, Z.-Y. Ge, Y. Wu, S. Wang, M. Gong, Y.-R. Zhang, Q. Zhu, R. Yang, S. Li, F. Liang, *et al.*, “Propagation and localization of collective excitations on a 24-qubit superconducting processor,” *Physical review letters*, vol. 123, no. 5, p. 050502, 2019.
 - [24] J. Carrasquilla, F. Becca, and M. Fabrizio, “Bose-glass, superfluid, and rung-mott phases of hard-core bosons in disordered two-leg ladders,” *Physical Review B*, vol. 83, no. 24, p. 245101, 2011.
 - [25] D. Jaksch, C. Bruder, J. I. Cirac, C. W. Gardiner, and P. Zoller, “Cold bosonic atoms in optical lattices,” *Physical Review Letters*, vol. 81, no. 15, p. 3108, 1998.
 - [26] M. Greiner, O. Mandel, T. Esslinger, T. W. Hänsch, and I. Bloch, “Quantum phase transition from a superfluid to a Mott insulator in a gas of ultracold atoms,” *Nature*, vol. 415, no. 6867, p. 39, 2002.
 - [27] N. Goldman and J. Dalibard, “Periodically driven quantum systems: effective Hamiltonians and engineered gauge fields,” *Physical review X*, vol. 4, no. 3, p. 031027, 2014.
 - [28] N. Goldman, J. Dalibard, M. Aidelsburger, and N. R. Cooper, “Periodically driven quantum matter: The case of resonant modulations,” *Physical Review A*, vol. 91, no. 3, p. 033632, 2015.
 - [29] F. Haldane, “Luttinger liquid theory of one-dimensional quantum fluids. i. properties of the luttinger model and their extension to the general 1d interacting spinless fermi gas,” *Journal of Physics C: Solid State Physics*, vol. 14, no. 19, p. 2585, 1981.
 - [30] T. Giamarchi, *Quantum physics in one dimension*, vol. 121. Clarendon press, 2003.
 - [31] D. J. Luitz, N. Laflorencie, and F. Alet, “Many-body localization edge in the random-field heisenberg chain,” *Physical Review B*, vol. 91, no. 8, p. 081103, 2015.
 - [32] A. Petrescu and K. Le Hur, “Chiral Mott insulators, Meissner effect, and Laughlin states in quantum ladders,” *Physical Review B*, vol. 91, no. 5, p. 054520, 2015.
 - [33] J. Schwinger, “Lectures on angular momentum,” in *Selected Papers on the Quantum Theory of Angular Momentum* (L. Biedenharn and H. van Dam, eds.), Academic Press, 1965.
 - [34] We assume (if not stated otherwise) for simplicity in the formulas that for all rungs j we have the magnetic vector potential such that $a'A_{\perp,i} = aA_{i,i+1}^{\parallel} = \phi$, i.e. we assume those two components to be equal and abbreviate them by a phase ϕ . At each site i , the perpendicular current and the outgoing parallel current are determined by the following operators [3].
 - [35] W. Meissner and R. Ochsenfeld, “Ein neuer Effekt bei Eintritt der Supraleitfähigkeit,” *Naturwissenschaften*, vol. 21, no. 44, pp. 787–788, 1933.
 - [36] E. Altman, W. Hofstetter, E. Demler, and M. D. Lukin, “Phase diagram of two-component bosons on an optical lattice,” *New Journal of Physics*, vol. 5, no. 1, p. 113, 2003.
 - [37] T. Senthil and M. P. A. Fisher, “ \mathbb{Z}_2 gauge theory of electron fractionalization in strongly correlated systems,” *Phys. Rev. B*, vol. 62, p. 7850, 2000.
 - [38] A. Kitaev and C. Laumann, “Lectures on topological phases and quantum computation,” in *Topological phases and quantum computation* (Arxiv:0904.2771, ed.), 2009.
 - [39] H. Schulz, “Fermi liquids and non-fermi liquids,” *arXiv preprint cond-mat/9503150*, 1995.
 - [40] A. Pal and D. A. Huse, “Many-body localization phase transition,” *Physical review b*, vol. 82, no. 17, p. 174411, 2010.
 - [41] J. H. Bardarson, F. Pollmann, and J. E. Moore, “Unbounded growth of entanglement in models of many-body localization,” *Physical review letters*, vol. 109, no. 1, p. 017202, 2012.
 - [42] E. Lieb, T. Schultz, and D. Mattis, “Two soluble models of an antiferromagnetic chain,” *Annals of Physics*, vol. 16, no. 3, pp. 407–466, 1961.
 - [43] Note that if Δ_+ and Δ_- both go to zero, we get a zero current, which is the case for the continuum limit. The interval $2\pi/L$ goes to zero and with that the amplitude of the current goes to zero as well.
 - [44] A. Luther and I. Peschel, “Single-particle states, kohn anomaly, and pairing fluctuations in one dimension,” *Physical Review B*, vol. 9, no. 7, p. 2911, 1974.
 - [45] E. Miranda, “Introduction to bosonization,” *Brazilian*

- Journal of Physics*, vol. 33, no. 1, pp. 3–35, 2003.
- [46] B. Chiaro *et al.*, “Direct measurement of non-local interactions in the many-body localized phase,” arXiv:1910.06024.
- [47] J. R. Johansson, P. Nation, and F. Nori, “Qutip: An open-source python framework for the dynamics of open quantum systems,” *Computer Physics Communications*, vol. 183, no. 8, pp. 1760–1772, 2012.